Hygro-thermal bending behavior of porous FG nano-beams via local/nonlocal strain and stress gradient theories of elasticity

Rosa PENNA, Luciano FEO, Giuseppe LOVISI

Department of Civil Engineering, University of Salerno, 84084, Fisciano, Italy

Key words: Porous Functionally Graded Materials, Nanobeams, Bending Behavior, Nonlocal Gradient Elasticity, Hygro-Thermo-Mechanical Loadings.

Abstract

This work studies the bending response of porous functionally graded Euler-Bernoulli nano-beams under hygro-thermo-mechanical loadings. The governing equations of the elastostatic problems associated with both local/nonlocal stress- and strain-driven gradient models of elasticity were derived by using the virtual work principle. A Wolfram language code in Mathematica was then written to carry out a numerical investigation for different boundary conditions including cantilever and simply-simply conditions. The effects of the different parameters, such as porosity volume fraction, gradient index, nonlocal parameter, gradient length parameter and mixture parameter are presented. It is shown how the proposed approach is able to capture the structural behavior of porous functionally graded Bernoulli–Euler nano-beams under a hygro-thermal environment.

1 Introduction

In recent years, nanostructures made of functionally graded materials (FGMs) have attracted a great deal of attention due to their wide range of applications in several fields of nanoscience as well as in various fields of engineering, such as automotive, chemical industry, energy, biomedical appliance, telecommunications and construction [1-11]. The latter field of application may be one of the main beneficiaries of this novel type of advanced composite materials, with applications that can improve either the characteristics of building elements surface, such as thermal insulation and fire protection, or the mechanical properties of conventional construction materials, such as the compressive strength and durability [12]. Moreover, due to their excellent energy absorption characteristics, FG materials with internal porosity have also been used in nanostructures under dynamic and impact loading [13-18].

It is well-known that the size-dependent response of nanostructures [19–20] may be predicted accurately by adopting scale-dependent continuum mechanics-based formulations, including Eringen's nonlocal theory [21, 22] and the nonlocal strain gradient elasticity developed by Lim et al [23] combining the strain gradient model [24, 25] and the Eringen's strain-driven integral formulation. Furthermore, the significant number of applications of FG materials under high temperature and absorbed moisture environments, such as aerospace and marine structures, has attracted particular attention from numerous scientists since the increase in temperature and humidity can lead to a reduction in their thermoelastic properties [26-31], thus resulting in a catastrophic failure of the structures. Therefore, some researchers have extended the above-mentioned theories to include the hygro-thermal effects. Relevant studies on this topic can be found in [32-37]. Although these theories have been used by many researchers to capture size effects in nanostructures, it has been claimed that both Eringen's nonlocal elasticity theory and Lim's nonlocal strain gradient elasticity, in their differential formulations, are not consistent when applied to finite structures and lead to ill-posed nanostructural problems. The ill-posedness of ENT is related to the fact that the higher-order constitutive boundary conditions are not compatible with the equilibrium requirements [38]. This problem can be overcome by using the stress-driven nonlocal model (SDM) proposed by Romano and Barretta in [39], which has been applied to solve relevant static, dynamic and buckling problems of nanomechanics [40-51]. Moreover, the application of Lim's approach leads to ill-posed structural problems since the constitutive boundary conditions are in conflict with both non-standard kinematic and static higher-order boundary conditions [52]. The ill-posedness of Lim's nonlocal strain gradient formulation can be advantageously bypassed using the methodology proposed by Barretta et al [53] in which the proper variational formulation of the elasto-static problem of nonlocal strain and stress gradient of inflected beams has been developed. The approach proposed by Barretta also offers a simple and effective strategy to predict the dynamic responses of modern composite nano-structures [54].

This study presents the results of a parametric investigation on the structural bending response of nano-beams made of porous functionally graded (FG) material under hygro-thermo-mechanical loadings, using both the local/nonlocal stress-driven (NStressG) and strain-driven (NStrainG) gradient models of elasticity. The numerical results obtained confirm that such formulations are able to fully capture the structural behavior of porous functionally graded Bernoulli−Euler nano-beams. These results are also important from the point of view of the design and optimization of

nanostructures susceptible to hygro-thermal stresses in the case of exposure to severe environmental conditions.

The paper is structured as follows. The effective mechanical and hygro-thermal properties of the FG material are presented in Section 2. Preliminary kinematic assumptions and the equations of equilibrium of Bernoulli–Euler nanobeams are derived in Section 3 by using the virtual work principle. In Section 4, both the local/nonlocal stress-driven and strain-driven gradient models of elasticity are introduced in order to obtain the governing equations of the elastostatic problem of a FG porous nano-beam exposed to hygro-thermal-mechanical loadings. The coupled effect of several parameters and hygrothermal loads on the structural response of two selected case-studies are presented in Section 5, in which the accuracy and the reliability of the proposed approach have also been assessed. Some closing remarks are provided in Section 6.

2 Functionally graded materials

Consider a nano-beam made of a metal-ceramic functionally graded material with length "*L*" undergoing hygro-thermal loads and denoted by *y'* and *z'* the principal axes of geometric inertia originating at the geometric center *O* of the nano-beam rectangular cross-section (Σ) with a thickness "*h*" and width "*b*", as shown in Figure 1.

Figure 1. Coordinate system and configuration of a porous FG Bernoulli-Euler nano-beam.

It is further assumed the nano-beam structure to have an even porosity distribution across the thickness, generated during its manufacturing process. Consequently, the effective mechanical and hygro-thermal properties of the FG material, here described by the mass density, $\rho(z')$, the Young's modulus, $E(z')$, the thermal expansions coefficient, $\alpha(z')$, and the moisture expansion coefficient, $\beta(z')$, can be calculated by the following rule of mixtures equations

$$\rho(z') = \rho_m + (\rho_c - \rho_m)\left(\frac{1}{2} + \frac{z'}{h}\right)^k - \frac{\zeta}{2}(\rho_c + \rho_m) \tag{1}$$

$$E(z') = E_m + (E_c - E_m)\left(\frac{1}{2} + \frac{z'}{h}\right)^k - \frac{\zeta}{2}(E_c + E_m) \tag{2}$$

$$\alpha(z') = \alpha_m + (\alpha_c - \alpha_m)\left(\frac{1}{2} + \frac{z'}{h}\right)^k - \frac{\zeta}{2}(\alpha_c + \alpha_m) \tag{3}$$

$$\beta(z') = \beta_m + (\beta_c - \beta_m)\left(\frac{1}{2} + \frac{z'}{h}\right)^k - \frac{\zeta}{2}(\beta_c + \beta_m) \tag{4}$$

where ρ_c, ρ_m and E_c, E_m are the material densities and the Euler-Young moduli of ceramic and metal, respectively; α_c, α_m and β_c, β_m are the thermal expansion coefficients and the moisture expansion coefficients of the two aforementioned materials, respectively. Furthermore, the symbols k ($k \geq 0$) and ζ ($\zeta < 1$) denote the gradient index and the porosity volume fraction of the FG material, respectively.

The characteristic values of the thermo-elastic properties, P_0, of metal (*SuS3O4*) and ceramic (*Si3N4*) are listed in Table 1 [26]. It is well-known that under an extreme temperature environment, the material properties are also assumed to be temperature-dependent by the following nonlinear equations

$$P(T) = P_0(1 + X_{-1}\,T^{-1} + X_1\,T + X_2\,T^2 + X_3\,T^3) \tag{5}$$

being X_{-1}, X_1, X_2 and X_3 the coefficients of material phases (Table 2).

In this investigation, both the uniform temperature rise (UTR) and linear temperature rise (LTR) between the bottom ($z'=-h/2$) and the top surface ($z'=+h/2$) of the nano-beam cross-section, are considered

- *UTR*

$$T(z') = T_b + \Delta T = const \tag{6}$$

- *LTR*

$$T(z') = T_b + \Delta T\left(\frac{z'}{h} + \frac{1}{2}\right) \tag{7}$$

while the moisture concentration is assumed to be constant through the thickness

$$C(z') = C_b + \Delta C = const \tag{8}$$

In Equations (6)-(8), $T(z')$ and $C(z')$ denote the current values of the temperature and moisture through the thickness direction (z'), respectively; T_b, C_b and T_t, C_t are the values of the temperature and moisture concentration at the bottom and top surface, respectively; $\Delta T = T_t - T_b$ and $\Delta C = C_t - -C_b$ denote the increments of the temperature and moisture concentration, respectively.

Table 1. Thermo-elastic properties of metal (*SuS3O4)* and ceramic (*Si3N4*).

Table 2. Coefficients of material phases for metal (*SuS3O4)* and ceramic (*Si3N4*).

In order to remove any bending–stretching coupling due to the variation of the functionally graded material, it is convenient to evaluate the effective thermo-elastic material properties (Equations (1)-(4)) with respect to the elastic center *C*, whose position, depending on the current value of the temperature *T*, is shifted from the geometric center *O* of the following quantity [51]

$$z_c' = \frac{\int_\Sigma E(z',T) z' d\Sigma}{\int_\Sigma E(z',T) d\Sigma} \tag{9}$$

In the new elastic Cartesian coordinate system, the coordinate *z* originating at *C* is given by $z = z' - z_c'$ and $y = y'$ (Figure 1). Consequently, the temperature-dependent bending and axial stiffnesses of the FG porous nano-beam, I_E and A_E, are expressed as follow

$$I_E = b \int_{-\frac{h}{2}-z_c'}^{\frac{h}{2}-z_c'} E(z,T) z^2 dz \tag{10}$$

$$A_E = b \int_{-\frac{h}{2}-z_c'}^{\frac{h}{2}-z_c'} E(z,T) dz \tag{11}$$

In the following, we show the effects of the porosity volume fraction (ζ) and the gradient index (k) on the dimensionless coordinate of the elastic centre ($\overline{z}_c' = z_c'/h$), as well as on the dimensionless bending $\left(\overline{I_E} = \frac{I_E}{I_{E_c}}\right)$ and dimensionless axial $\left(\overline{A_E} = \frac{A_E}{A_{E_c}}\right)$ stiffnesses of Σ, varying the temperature distribution. It is worth noting that I_{E_c} and A_{E_c} represent, respectively, the bending and the axial stiffnesses of a non-porous purely ceramic nano-beam.

For a better mechanical and physical interpretation of the subsequent results, in Table 3 we summarize the thermo-elastic parameters of metal (*SuS3O4)* and ceramic (*Si3N4*) evaluated for four values of the temperature (T=305, 405, 505, 605 [K]).

Table 3. Thermo-elastic properties of metal (*SuS3O4)* and ceramic (*Si3N4*) at different temperatures.

Figures 2 plot the effects of the gradient index on the dimensionless position $\overline{z}_c'$ of the elastic centre *C* for both non-porous ($\zeta = 0.0$) and porous ($\zeta = 0.25$) FG nano-beams under four different uniform (a) and linear (b) temperature rises (namely ΔT=0, 100, 200, 300 [K]) starting from an initial value of the bottom surface temperature, T_b , equal to 305 [K].

Firstly, it can be observed that the curves of the dimensionless coordinate $\overline{z}_c'$ increase as k increases, and reach a maximum value depending on ζ and ΔT. In particular, it is found that as ΔT increases the values of $\overline{z}_c'$ corresponding to the uniform thermal distribution (Figure 2a) are always greater than those obtained for $\Delta T = 0$, for both non-porous and porous FG nano-beams, while an opposite trend has been obtained in the case of linear thermal distributions (Figure 2b).

The dimensionless position of the elastic centre *C* versus the porosity volume fraction is presented in Figures 3 varying the material gradient index *k* in the set {0.3, 1.0, 3.0} and considering both the uniform (a) and linear (b) temperature rises. As it can be observed, the dimensionless position of *C* always increases as ζ increases. Moreover, in the case of the uniform thermal distribution, the increase in temperature leads to an increase of the value of $\overline{z}_c'$ for all the values of *k* (Figure 3a). On the contrary, an opposite and less sensitive tendency was obtained for linear thermal distributions (Figure 3b).

Figures 4 show the variations of the dimensionless bending, $\overline{I_E}$, and axial stiffnesses, $\overline{A_E}$, for non-porous and porous FG nano-beam under both uniform and linear thermal distributions. As can be noted, these quantities decrease as the material gradient index and the porosity index increase for all the temperature values. The same effect is observed upon increasing the temperature, but its influence is more evident in the case of uniform thermal distributions (Figures 4a and 4c). The effect of porosity on the mechanical properties of the FG nano-beam is even more evident from the graphs of Figures 5, where the curves of the dimensionless bending and axial stiffnesses are plotted for three different values of the gradient index (*k=0.3,1.0,3.0*). In fact, as ζ and *k* increase, the values of the dimensionless stiffnesses decrease for both the uniform (Figures 5a and 5c) and linear (Figures 5b and 5d) thermal distributions. Finally, Figures 6 shows the temperature effects on $\overline{I_E}$ and $\overline{A_E}$ for non-porous and porous FG materials upon varying the gradient index in the set (*0.3,1.0,3.0*). It should be noted that, within the range of the values of temperature increments here considered (ΔT=0, 100, 200, 300 [K]), the dimensionless bending and axial stiffnesses decrease as ΔT increases. Moreover, the

presence of an even distribution of porosity determines a significant abatement of the mechanical properties of the nano-beam.

Figures 2. Effects of the gradient index (*k*) on the dimensionless position of the elastic centre *C* for non-porous ($\zeta = 0.0$) and porous ($\zeta = 0.25$) FG materials under uniform (a) and linear (b) temperature rises (ΔT=0, 100, 200, 300 [K]).

Figures 3. Effects of the porosity volume fraction (ζ) on the dimensionless position of the elastic centre *C* for three different values of the material gradient index (*k=0.3,1.0,3.0*) under uniform (a) and linear (b) temperature rises (ΔT=0, 300 [K]).

Figures 4. Effects of the gradient index (*k*) on the dimensionless bending stiffness $\overline{I_E}$ (a,b) and axial stiffness $\overline{A_E}$ (c,d) for non-porous ($\zeta = 0.0$) and porous ($\zeta = 0.25$) FG materials under uniform (a,c) and linear (b,d) temperature rises (ΔT=0, 100, 200, 300 [K]).

Figures 5. Effects of the porosity volume fraction (ζ) on the dimensionless bending stiffness $\overline{I_E}$ (a,b) and axial stiffness $\overline{A_E}$ (c,d) for three different values of the gradient index (*k=0.3,1.0,3.0*) of the FG material under uniform (a,c) and linear (b,d) temperature rises (ΔT=0, 300 [K]).

Figures 6. Effects of uniform (a,c) and linear (b,d) temperature rises on the dimensionless bending stiffness $\overline{I_E}$ (a, b) and axial stiffness $\overline{A_E}$ (c, d) for non-porous ($\zeta = 0.0$) and porous ($\zeta = 0.25$) FG materials and for three different values of the gradient index (*k=0.3,1.0,3.0*).

3 Governing equations

Based on Bernoulli-Euler theory, in the elastic coordinate reference system $\{C, x, y, z\}$, the Cartesian components of the displacement field of the nano-beam, u_x, u_y and u_z, along *x*, *y* and *z* directions, respectively, can be expressed as

$$u_x(x,z) = u(x) - z\frac{\partial w}{\partial x}(x) \tag{12}$$

$$u_y(x,z) = 0 \tag{13}$$

$$u_z(x,z) = w(x) \tag{14}$$

where $u(x)$ and $w(x)$ are the axial and transverse displacements of the elastic centre C, respectively. Consequently, the only nonzero component deformation associated with the displacement field is the (total) axial strain, defined as

$$\varepsilon_{xx} = \frac{\partial u}{\partial x} - z\frac{\partial^2 w}{\partial x^2} \tag{15}$$

By using the principle of virtual work, we can derive the governing equations, as follows

$$\delta U + \delta W = 0 \tag{16}$$

being δU and δW the virtual strain energy and the virtual work done by external forces, respectively.

The first variation of the strain energy δU is given by

$$\delta U = \int_0^L \int_\Sigma \sigma_{xx}\, \delta\varepsilon_{xx}\, d\Sigma\, dx = \int_0^L \left(N\left(\frac{\partial \delta u}{\partial x}\right) - M\left(\frac{\partial^2 \delta w}{\partial x^2}\right)\right) dx \tag{17}$$

where $\sigma_{xx} = \sigma_{xx}(z,T) = E(z,T)\, \varepsilon_{xx} = E\, \varepsilon_{xx}$, is the temperature-dependent axial stress, and N and M, are the axial and moment stress resultants, respectively

$$N = \int_\Sigma \sigma_{xx}\, d\Sigma \tag{18}$$

$$M = \int_\Sigma z\, \sigma_{xx}\, d\Sigma \tag{19}$$

The expression of the virtual work of the external force δW can be expressed by

$$\delta W = -\int_0^L \left(q_x\, \delta u + q_z \delta w + (N^T + N^C) \frac{\partial w}{\partial x} \frac{\partial \delta w}{\partial x} \right) dx \tag{20}$$

where $q_x = q_x(x)$ and $q_z = q_z(x)$ are the axial and transverse vertical distributed loads, respectively; N^T and N^C denote the hygro-thermal axial force resultants, defined as follow

$$N^T = N^T(z,T) = \int_\Sigma E\alpha\Delta T dz \tag{21}$$

$$N^C = N^C(z,T) = \int_\Sigma E\beta\Delta C dz \tag{22}$$

in which $\alpha = \alpha(z,T)$ and $\beta = \beta(z,T)$ are the thermal and moisture expansion temperature-dependent coefficients, respectively, defined previously.

By substituting Equations (17) and (20) into Equation (16), and using the fundamental lemma of variational calculus, the following equations of equilibrium can be obtained:

$$\frac{\partial N}{\partial x} + q_x = 0 \tag{23}$$

$$\frac{\partial^2 M}{\partial x^2} + q_z - (N^T + N^C)\frac{\partial^2 w}{\partial x^2} = 0 \tag{24}$$

The corresponding boundary conditions at the nano-beam's ends ($x = 0$ and $x = L$) can be chosen by specifying one element of each of the following three pairs (standard kinematic or static boundary conditions, SBC)

$$u \text{ or } N \tag{25}$$

$$-\frac{\partial w}{\partial x} \text{ or } M \tag{26}$$

$$w \text{ or } \frac{\partial M}{\partial x} - (N^T + N^C)\frac{\partial w}{\partial x} \tag{27}$$

4. Local/Nonlocal gradient formulation

The abstract formulation of local/nonlocal gradient elasticity is expressed by the following integro-differential law relating a source field, $s(x)$: $[0, L] \rightarrow R$, and an output field, $f(x)$: $[0, L] \rightarrow R$ [53]

$$f(x) = \xi_1\, s(x) + \xi_2 \int_0^L \Phi_{L_c}(x-\xi)\, \mathrm{s}(\xi) d\xi - L_l^2 \frac{\partial}{\partial x}\int_0^L \Phi_{L_c}(x-\xi)\, \frac{\partial\, \mathrm{s}(\xi)}{\partial x} d\xi \tag{28}$$

where Φ_{L_c} is the scalar averaging kernel, depending on the length-scale parameter, L_c, which describes the nonlocal effects; L_l denotes the gradient length parameter, introduced to capture the effects of the higher-order axial strain; ξ_1 and ξ_2 are the two phase parameters.

It is well-known how the aforementioned constitutive mixture equation can be seen as the competition between the classical local elasticity (with volume fraction ξ_1) and the nonlocal elasticity (with volume fraction ξ_2) where the two-phase parameters must fulfil the conditions: $0 < (\xi_1, \xi_2) < 1$ and $\xi_1 + \xi_2 = 1$. Thus, the gradient nonlocal law is obtained by setting $\xi_1 = 0$ (or $\xi_2 = 1$), while the well-known classical local gradient law corresponds to $\xi_1 = 1$ (or $\xi_2 = 0$).

In the following paragraphs, both the local/nonlocal stress-driven and strain-driven gradient models of elasticity are introduced in order to obtain the governing equations of the elastostatic problem of a FG porous nano-beam exposed to a hygro-thermal rise.

4.1 Stress gradient formulation (NStressG)

Local/nonlocal stress gradient formulation is obtained by setting in the Equation (28) the source field, $s(x) = \frac{\sigma_{xx}(x)}{E}$ and the output field $f(x) = \varepsilon_{xx}^{el}$, being σ_{xx} the axial stress component, subjected to equilibrium conditions, and ε_{xx}^{el} the elastic axial strain component.

It follows that Equation (28) is transformed into the following local/nonlocal constitutive mixture equation, expressing the elastic axial strain as the function of strains at both the reference point x and its nearby points ξ

$$\varepsilon_{xx}^{el} = \xi_1 \frac{\sigma_{xx}(x)}{E} + \frac{\xi_2}{E} \int_0^L \Phi_{L_c}(x-\xi)\, \sigma_{xx}(\xi) d\xi - \frac{1}{E} L_l^2 \frac{\partial}{\partial x} \int_0^L \Phi_{L_c}(x-\xi) \frac{\partial \sigma_{xx}(\xi)}{\partial x} d\xi \tag{29}$$

where $\frac{\partial \sigma_{xx}}{\partial_x}$ denotes the gradient of the axial stress component.

In a hygrothermal environment, the elastic axial strain is expressed as the difference between the total strain, ε_{xx}, and the non-elastic axial strain, $\varepsilon_{xx}^{*} = \alpha\, \Delta T + \beta \Delta C$, depending on the increases in temperature, ΔT, and moisture concentration, ΔC, (i.e. hygrothermal effects)

$$\varepsilon_{xx}^{el} = \varepsilon_{xx} - \varepsilon_{xx}^{*} \tag{30}$$

Choosing the bi-exponential function for the kernel Φ_{L_c} as

$$\Phi_{L_c}(x, L_c) = \frac{1}{2L_c} \exp\left(-\frac{|x|}{L_c}\right) \tag{31}$$

and substituting the relations $\xi_2 = 1 - \xi_1$, the integro-differential relation of Equation (29) admit the following set of solutions

$$\varepsilon_{xx}^{el} - L_c^2 \frac{\partial^2 \varepsilon_{xx}^{el}}{\partial x^2} = \frac{\sigma_{xx}}{E} - \frac{L_c^2}{E}\left(\xi_1 + \frac{L_l^2}{L_c^2}\right) \frac{\partial^2 \sigma_{xx}}{\partial x^2} \tag{32}$$

with $x \in [0, L]$, if and only if the following two pairs of constitutive boundary conditions (CBCs) are satisfied at the nano-beam ends:

$$\frac{\partial \varepsilon_{xx}^{el}(0)}{\partial x} - \frac{1}{L_c}\varepsilon_{xx}^{el}(0) = -\frac{1}{E}\frac{\xi_1}{L_c}\sigma_{xx}(0) + \frac{1}{E}\left(\xi_1 + \frac{L_l^2}{L_c^2}\right)\frac{\partial \sigma_{xx}(0)}{\partial x} \tag{33}$$

$$\frac{\partial \varepsilon_{xx}^{el}(L)}{\partial x} + \frac{1}{L_c}\varepsilon_{xx}^{el}(L) = \frac{1}{E}\frac{\xi_1}{L_c}\sigma_{xx}(L) + \frac{1}{E}\left(\xi_1 + \frac{L_l^2}{L_c^2}\right)\frac{\partial \sigma_{xx}(L)}{\partial x} \tag{34}$$

By manipulating Equations (15) and (30) and substituting into Equations (32)-(34), then multiplying by (1, z), the integration over the nano-beam cross section provides the following NStressG equations in terms of axial and transverse displacement

$$\mathrm{A_E}\frac{\partial u}{\partial x} - A_E L_c^2 \frac{\partial^3 u}{\partial x^3} - N^T - N^C = N^{NStressG} - L_c^2\left(\xi_1 + \frac{{L_l}^2}{{L_c}^2}\right)\frac{\partial^2 N^{NStressG}}{\partial x^2} \tag{35}$$

$$-I_E\frac{\partial^2 w}{\partial x^2} + I_E L_c^2\frac{\partial^4 w}{\partial x^4} - M^T - M^C = M^{NStressG} - L_c^2\left(\xi_1 + \frac{{L_l}^2}{{L_c}^2}\right)\frac{\partial^2 M^{NStressG}}{\partial x^2} \tag{36}$$

with the corresponding constitutive boundary conditions (at $x = 0, L$)

$$A_E\left(\frac{\partial^2 u(0)}{\partial x^2} - \frac{1}{L_c}\frac{\partial u(0)}{\partial x}\right) = -\frac{\xi_1}{L_c}N^{NStressG}(0) + \left(\xi_1 + \frac{L_l^2}{L_c^2}\right)\frac{\partial N^{NStressG}(0)}{\partial x} \tag{37}$$

$$A_E\left(\frac{\partial^2 u(L)}{\partial x^2} + \frac{1}{L_c}\frac{\partial u(L)}{\partial x}\right) = \frac{\xi_1}{L_c}N^{NStressG}(L) + \left(\xi_1 + \frac{L_l^2}{L_c^2}\right)\frac{\partial N^{NStressG}(L)}{\partial x} \tag{38}$$

$$-I_E\frac{\partial^3 w(0)}{\partial x^3} + \frac{1}{L_c}I_E\frac{\partial^2 w(0)}{\partial x^2} = -\frac{\xi_1}{L_c}M^{NStressG}(0) + \left(\xi_1 + \frac{L_l^2}{L_c^2}\right)\frac{\partial M^{NStressG}(0)}{\partial x} \tag{39}$$

$$-I_E\frac{\partial^3 w(L)}{\partial x^3} - \frac{1}{L_c}I_E\frac{\partial^2 w(L)}{\partial x^2} = \frac{\xi_1}{L_c}M^{NStressG}(L) + \left(\xi_1 + \frac{L_l^2}{L_c^2}\right)\frac{\partial M^{NStressG}(L)}{\partial x} \tag{40}$$

in which $N^{NStressG}$ and $M^{NStressG}$ denote the stress gradient axial force and moment resultants, respectively; N^T and N^C are the hygro-thermal axial force resultants previously defined in Equation (21) and Equation (22), respectively; M^T and M^C can be defined as the hygro-thermal bending moment resultants, as

$$M^T = M^T(z,T) = \int_{\Sigma} E\alpha\Delta T z dz \tag{41}$$

$$M^C = M^C(z,T) = \int_{\Sigma} E\beta\Delta C z dz \tag{42}$$

which are null with respect to a coordinate system originating at the elastic centre *C*.

Substituting Equations (23) and (24) into Equations (35) and (36), the nonlocal stress gradient axial force and moment resultants can be expressed as follows

$$N^{NStressG} = A_E \frac{\partial u}{\partial x} - A_E L_c^{\mathbf{2}} \frac{\partial^3 u}{\partial x^3} - N^T - N^C - L_c^2 \left(\xi_1 + \frac{L_l^{\,2}}{L_c^{\mathbf{2}}}\right) \frac{\partial q_x}{\partial x} \tag{43}$$

$$M^{NStressG} = -I_E \frac{\partial^2 w}{\partial x^2} + I_E L_c^{\mathbf{2}} \frac{\partial^4 w}{\partial x^4} - M^T - M^C + L_c^2 \left(\xi_1 + \frac{L_l^{\,2}}{L_c^{\mathbf{2}}}\right)\left(-q_z + (N^T + N^C)\frac{\partial^2 w}{\partial x^2}\right) \tag{44}$$

By manipulating Equations (43, 44) and Equations (23, 24), gives the following NStressG ordinary differential governing equations in terms of displacement

$$-A_E L_c^2 \frac{\partial^4 u}{\partial x^4} + A_E \frac{\partial^2 u}{\partial x^2} - \frac{\partial N^T}{\partial x} - \frac{\partial N^C}{\partial x} - L_c^2 \left(\xi_1 + \frac{L_l^{\,2}}{L_c^2}\right) \frac{\partial^2 q_x}{\partial x^2} + q_x = 0 \tag{45}$$

$$I_E L_c^2 \frac{\partial^6 w}{\partial x^6} - I_E \frac{\partial^4 w}{\partial x^4} - \frac{\partial^2 M^T}{\partial x^2} - \frac{\partial^2 M^C}{\partial x^2} + L_c^2 \left(\xi_1 + \frac{L_l^{\,2}}{L_c^2}\right) \frac{\partial^2}{\partial x^2}\left((N^T + N^C)\frac{\partial^2 w}{\partial x^2} - q_z\right) - (N^T + N^C)\frac{\partial^2 w}{\partial x^2} + q_z = 0 \tag{46}$$

equipped with the kinematic and static boundary conditions imposed by Equations (25)-(27) and the constitutive boundary conditions (CBCs) expressed by Equations (37)-(40).

4.2 Strain gradient formulation (NStrainG)

Local/nonlocal strain gradient formulation is obtained by setting in Equation (28) the source field, $s(x) = \varepsilon_{xx}^{el}$ and the output field $f(x) = \frac{\sigma_{xx}(x)}{E}$. It follows that Equation (28) is transformed into the following local/nonlocal constitutive mixture NStrainG formulation

$$\frac{\sigma_{xx}(x)}{E} = \xi_1 \varepsilon_{xx}^{el} + \xi_2 \int_0^L \Phi_{L_c}(x-\xi)\, \varepsilon_{xx}^{el}(\xi) d\xi - L_l^2 \frac{\partial}{\partial x} \int_0^L \Phi_{L_c}(x-\xi) \frac{\partial \varepsilon_{xx}^{el}(\xi)}{\partial x} d\xi \tag{47}$$

Equation (47) is equivalent to the following differential law

$$\sigma_{xx} - L_c^2 \frac{\partial^2 \sigma_{xx}}{\partial x^2} = E\,(\varepsilon_{xx} - \alpha \Delta T - \beta \Delta C) - E L_c^2 \left(\xi_1 + \frac{L_l^2}{L_c^2}\right) \frac{\partial^2 \varepsilon_{xx}}{\partial x^2} \tag{48}$$

equipped with the following two pairs of constitutive boundary conditions

$$\frac{\partial \sigma_{xx}(0)}{\partial x} - \frac{1}{L_c}\sigma_{xx}(0) = -E \frac{\xi_1}{\boldsymbol{L_c}} \varepsilon_{xx}(0) + E \left(\xi_1 + \frac{L_l^2}{L_c^2}\right) \frac{\partial \varepsilon_{xx}(0)}{\partial x} \tag{49}$$

$$\frac{\partial \sigma_{xx}(L)}{\partial x} + \frac{1}{L_c}\sigma_{xx}(L) = E\frac{\xi_1}{\boldsymbol{L_c}}\varepsilon_{xx}(L) + E\left(\xi_1 + \frac{L_l^2}{L_c^2}\right)\frac{\partial \varepsilon_{xx}(L)}{\partial x} \tag{50}$$

By repeating the same steps developed in the previous paragraph related to the stress gradient formulation, the following NStrainG ordinary differential governing equations are obtained

$$A_E\frac{\partial^2 u}{\partial x^2} - \frac{\partial N^T}{\partial x} - \frac{\partial N^C}{\partial x} - L_c^2\frac{\partial^2 q_x}{\partial x^2} - A_E L_c^2\left(\xi_1 + \frac{L_l^2}{L_c^2}\right)\frac{\partial^4 u}{\partial x^4} + q_x = 0 \tag{51}$$

$$-I_E\frac{\partial^4 w}{\partial x^4} + L_c^2\frac{\partial^2}{\partial x^2}\left((N^T + N^C)\frac{\partial^2 w}{\partial x^2}\right) - \frac{\partial^2 M^T}{\partial x^2} - \frac{\partial^2 M^C}{\partial x^2} - L_c^2\frac{\partial^2 q_x}{\partial x^2} + I_E L_c^2\left(\xi_1 + \frac{L_l^2}{L_c^2}\right)\frac{\partial^6 w}{\partial x^6} + q_z - (N^T + N^C)\frac{\partial^2 w}{\partial x^2} = 0 \tag{52}$$

which can be solved by prescribing the standard boundary conditions (SBC) expressed by Equations (25)-(27) and the following constitutive ones at $x = 0, L$ (CBC)

$$\frac{\partial N^{NStrainG}}{\partial x}(0) - \frac{1}{L_c}N^{NStrainG}(0) = -\frac{\xi_1}{L_c}A_E\frac{\partial u}{\partial x}(0) + A_E\left(\xi_1 + \frac{L_l^2}{L_c^2}\right)\frac{\partial^2 u}{\partial x^2}(0) \tag{53}$$

$$\frac{\partial N^{NStrainG}}{\partial x}(L) + \frac{1}{L_c}N^{NStrainG}(L) = \frac{\xi_1}{L_c}A_E\frac{\partial u}{\partial x}(0) + A_E\left(\xi_1 + \frac{L_l^2}{L_c^2}\right)\frac{\partial^2 u}{\partial x^2}(0) \tag{54}$$

$$\frac{\partial M^{NStrainG}}{\partial x}(0) - \frac{M^{NStrainG}}{L_C}(0) = \frac{\xi_1}{L_c}I_E\frac{\partial^2 w}{\partial x^2}(0) - I_E\left(\xi_1 + \frac{L_l^2}{L_c^2}\right)\frac{\partial^3 w}{\partial x^3}(0) \tag{55}$$

$$\frac{\partial M^{NStrainG}}{\partial x}(L) + \frac{M^{NStrainG}}{L_C}(L) = -\frac{\xi_1}{L_c}I_E\frac{\partial^2 w}{\partial x^2}(L) - I_E\left(\xi_1 + \frac{L_l^2}{L_c^2}\right)\frac{\partial^3 w}{\partial x^3}(L) \tag{56}$$

where the expressions of $N^{NStrainG}$ and $M^{NStrainG}$ are reported in the following equations

$$N^{NStrainG} = A_E\frac{\partial u}{\partial x} - L_c^2\frac{\partial q_x}{\partial x} - N^T - N^C - A_E L_c^2\left(\xi_1 + \frac{L_l^2}{L_c^2}\right)\frac{\partial^3 u}{\partial x^3} \tag{57}$$

$$M^{NStrainG} = -I_E\frac{\partial^2 w}{\partial x^2} + L_c^2(N^T + N^c)\frac{\partial^2 w}{\partial x^2} - L_c^2 q_z - M^T - M^C + I_E L_c^2\left(\xi_1 + \frac{L_l^2}{L_c^2}\right)\frac{\partial^4 w}{\partial x^4} \tag{58}$$

4.3 Statics of inflected porous FG nano-beams

In this section, the dimensionless equations governing the elastic equilibrium of NStressG and NStrainG inflected beams are obtained.

By introducing the following dimensionless quantities

$$\tilde{x} = \frac{x}{L}$$
$$\widetilde{w} = \frac{w}{L}$$
$$\widetilde{M} = \frac{\bar{M}}{I_E}L$$
$$\tilde{V} = \frac{\bar{V}}{I_E}L^2$$
$$\widetilde{q_z} = \frac{q_z}{I_E}L^3$$
$$\lambda_c = \frac{L_c}{L}$$
$$\lambda_l = \frac{L_l}{L}$$
$$\widetilde{N^T} = \frac{N^T}{I_E}L^2$$
$$\widetilde{N^C} = \frac{N^C}{I_E}L^2$$
$$\widetilde{M^T} = \frac{M^T}{I_E}L$$
$$\widetilde{M^C} = \frac{M^C}{I_E}L \tag{59}$$

the dimensionless equations of the elastostatic problems associated with NStressG and NStrainG inflected beams can be formulated as follows.

4.3.1. Elastostatic problem of NStressG inflected nano-beams

Equilibrium equation

$$\lambda_c^2\frac{\partial^6\widetilde{w}(\tilde{x})}{\partial\tilde{x}^6} - \frac{\partial^4\widetilde{w}(\tilde{x})}{\partial\tilde{x}^4} - \frac{\partial^2\widetilde{M^T}}{\partial\tilde{x}^2} - \frac{\partial^2\widetilde{M^C}}{\partial\tilde{x}^2} + \lambda_c^2\left(\xi_1 + \frac{\lambda_l^2}{\lambda_c^2}\right)\frac{\partial^2}{\partial x^2}\left(\left(\widetilde{N^T} + \widetilde{N^C}\right)\frac{\partial^2\widetilde{w}(\tilde{x})}{\partial\tilde{x}^2} - \widetilde{q_z}\right) - \left(\widetilde{N^T} + \widetilde{N^C}\right)\frac{\partial^2\widetilde{w}(\tilde{x})}{\partial\tilde{x}^2} + \widetilde{q_z} = 0 \tag{60}$$

Standard boundary conditions

$$\widetilde{w}(\tilde{x}) = \widetilde{w^*} \quad \text{or} \quad \frac{\partial\widetilde{M}^{NStressG}(\tilde{x})}{\partial\tilde{x}} - \left(\widetilde{N^T} + \widetilde{N^C}\right)\frac{\partial\widetilde{w}(\tilde{x})}{\partial\tilde{x}} = \tilde{V} \tag{61}$$

$$-\frac{\partial\widetilde{w}(\tilde{x})}{\partial\tilde{x}} = \frac{\partial\widetilde{w}^*}{\partial\tilde{x}} \quad \text{or} \quad \widetilde{M}^{NStressG}(\tilde{x}) = \widetilde{M} \tag{62}$$

Constitutive boundary conditions

$$-\frac{\partial^3\widetilde{w}(0)}{\partial\tilde{x}^3}+\frac{1}{\boldsymbol{\lambda_c}}\frac{\partial^2\widetilde{w}(0)}{\partial\tilde{x}^2}=-\frac{\xi_1}{\boldsymbol{\lambda_c}}\widetilde{M}^{NStressG}(0)+\left(\xi_1+\frac{\boldsymbol{\lambda_l^2}}{\boldsymbol{\lambda_c^2}}\right)\frac{\partial\widetilde{M}^{NStressG}(0)}{\partial\tilde{x}} \tag{63}$$

$$-\frac{\partial^3\widetilde{w}(1)}{\partial\tilde{x}^3}-\frac{1}{\boldsymbol{\lambda_c}}\frac{\partial^2\widetilde{w}(1)}{\partial\tilde{x}^2}=\frac{\xi_1}{\boldsymbol{\lambda_c}}\widetilde{M}^{NStressG}(1)+\left(\xi_1+\frac{\boldsymbol{\lambda_l^2}}{\boldsymbol{\lambda_c^2}}\right)\frac{\partial\widetilde{M}^{NStressG}(1)}{\partial\tilde{x}} \tag{64}$$

being

$$\widetilde{M}^{NStressG}=-\frac{\partial^2\widetilde{w}(\tilde{x})}{\partial\tilde{x}^2}+\lambda_c^2\frac{\partial^4\widetilde{w}(\tilde{x})}{\partial\tilde{x}^4}-\widetilde{M}^T-\widetilde{M}^C+\lambda_c^2\left(\xi_1+\frac{\lambda_l{}^2}{\lambda_c{}^2}\right)\left(\left(\widetilde{N}^T+\widetilde{N}^C\right)\frac{\partial^2\widetilde{w}(\tilde{x})}{\partial\tilde{x}^2}-\tilde{q}_z\right) \tag{65}$$

4.3.2. Elastostatic problem of NStrainG inflected nano-beams

Equilibrium equation

$$-\frac{\partial^4\widetilde{w}(\tilde{x})}{\partial\tilde{x}^4}-\lambda_c^2\frac{\partial^2\widetilde{q}_z}{\partial\tilde{x}^2}+\lambda_c^2\frac{\partial^2}{\partial\tilde{x}^2}\left(\left(\widetilde{N^T}+\widetilde{N^C}\right)\frac{\partial^2\widetilde{w}(\tilde{x})}{\partial\tilde{x}^2}\right)-\frac{\partial^2\widetilde{M^T}}{\partial\tilde{x}^2}-\frac{\partial^2\widetilde{M^C}}{\partial\tilde{x}^2}+\lambda_c^2\left(\xi_1+\frac{\lambda_l^2}{\lambda_c^2}\right)\frac{\partial^6\widetilde{w}(\tilde{x})}{\partial\tilde{x}^6}-\left(\widetilde{N^T}+\widetilde{N^C}\right)\frac{\partial^2\widetilde{w}(\tilde{x})}{\partial\tilde{x}^2}+\tilde{q}_z=0 \tag{66}$$

Standard boundary conditions

$$\widetilde{w}(\tilde{x})=\widetilde{w^*}\quad\text{or}\quad\frac{\partial\widetilde{M}^{NStrainG}(\tilde{x})}{\partial\tilde{x}}-\left(\widetilde{N^T}+\widetilde{N^C}\right)\frac{\partial\widetilde{w}(\tilde{x})}{\partial\tilde{x}}=\tilde{V} \tag{67}$$

$$-\frac{\partial\widetilde{w}(\tilde{x})}{\partial\tilde{x}}=\frac{\partial\widetilde{w}^*}{\partial\tilde{x}}\quad\text{or}\quad\widetilde{M}^{NStrainsG}(\tilde{x})=\widetilde{M} \tag{68}$$

Constitutive boundary conditions

$$\frac{\partial\widetilde{M}^{NStrainG}(0)}{\partial\tilde{x}}-\frac{\widetilde{M}^{NStrainG}(0)}{\boldsymbol{\lambda_c}}=\frac{\xi_1}{\lambda_c}\frac{\partial^2\widetilde{w}(0)}{\partial\tilde{x}}-\left(\xi_1+\frac{\lambda_l{}^2}{\lambda_c^2}\right)\frac{\partial^3\widetilde{w}(0)}{\partial\tilde{x}^3} \tag{69}$$

$$\frac{\partial\widetilde{M}^{NStrainG}(1)}{\partial\tilde{x}}+\frac{\widetilde{M}^{NStrainG}(1)}{\boldsymbol{\lambda_c}}=-\frac{\xi_1}{\boldsymbol{\lambda_c}}\frac{\partial^2\widetilde{w}(1)}{\partial\tilde{x}}-\left(\xi_1+\frac{\lambda_l{}^2}{\boldsymbol{\lambda_c^2}}\right)\frac{\partial^3\widetilde{w}(1)}{\partial\tilde{x}^3} \tag{70}$$

being

$$\widetilde{M}^{NStrainG}=-\frac{\partial^2\widetilde{w}(\tilde{x})}{\partial\tilde{x}^2}+\lambda_c^2\left(\left(\widetilde{N}^T+\widetilde{N}^C\right)\frac{\partial^2\widetilde{w}(\tilde{x})}{\partial\tilde{x}^2}-\tilde{q}_z\right)-\widetilde{M}^T-\widetilde{M}^C+\lambda_c^2\left(\xi_1+\frac{\lambda_l{}^2}{\lambda_c{}^2}\right)\frac{\partial^4\widetilde{w}(\tilde{x})}{\partial\tilde{x}^4} \tag{71}$$

By setting $\xi_1=0$ and $\lambda_l=0$ in Equation (60), we get the differential equation of a purely nonlocal stress-driven model [39] in a hygro-thermal environment

- *Nonlocal Stress-Driven model*

$$\lambda_c^2 \frac{\partial^6 \widetilde{w}(\tilde{x})}{\partial \tilde{x}^6} - \frac{\partial^4 \widetilde{w}(\tilde{x})}{\partial \tilde{x}^4} - \frac{\partial^2 \widetilde{M}^T}{\partial \tilde{x}^2} - \frac{\partial^2 \widetilde{M}^C}{\partial \tilde{x}^2} - \left(\widetilde{N}^T + \widetilde{N}^C\right) \frac{\partial^2 \widetilde{w}(\tilde{x})}{\partial \tilde{x}^2} + \tilde{q}_z = 0 \tag{72}$$

with the following boundary conditions (at $\tilde{x} = 0, 1$)

$$\frac{\partial^3 \widetilde{w}}{\partial \tilde{x}^3}(0) = \frac{1}{\lambda_c} \frac{\partial^2 \widetilde{w}}{\partial \tilde{x}^2}(0) \tag{73}$$

$$\frac{\partial^3 \widetilde{w}}{\partial \tilde{x}^3}(1) = -\frac{1}{\lambda_c} \frac{\partial^2 \widetilde{w}}{\partial \tilde{x}^2}(1) \tag{74}$$

Moreover, by setting $\xi_1 = 0$ and $\lambda_l = 0$ in Equation (66), we get the differential equation of Eringen's nonlocal strain-driven model [22] in a hygro-thermal environment

- *Nonlocal Strain-Driven model*

$$-\frac{\partial^4 \widetilde{w}(\tilde{x})}{\partial \tilde{x}^4} + \lambda_c^2 \frac{\partial^2}{\partial \tilde{x}^2}\left(\left(\widetilde{N}^T + \widetilde{N}^C\right) \frac{\partial^2 \widetilde{w}(\tilde{x})}{\partial \tilde{x}^2}\right) - \lambda_c^2 \frac{\partial^2 \tilde{q}_z}{\partial \tilde{x}^2} - \frac{\partial^2 \widetilde{M}^T}{\partial \tilde{x}^2} - \frac{\partial^2 \widetilde{M}^C}{\partial \tilde{x}^2} - \left(\widetilde{N}^T + \widetilde{N}^C\right) \frac{\partial^2 \widetilde{w}(\tilde{x})}{\partial \tilde{x}^2} + \tilde{q}_z = 0 \tag{75}$$

with the following boundary conditions (at $\tilde{x} = 0, 1$).

5. Results and discussion

A numerical investigation on the bending response of FG porous Bernoulli-Euler nano-beams has been developed considering two static schemes: a cantilever (C-F) nano-beam, subjected to a concentrated load, $\tilde{V} = 1$, at the free dimensionless abscissa ($\tilde{x} = 1$), and a simply supported (S-S) nano-beam under the uniformly distributed dimensionless load, $\widetilde{q_z} = 1$, across the complete span, as illustrated in Figure 7. The analysis has been conducted using both local/nonlocal strain and stress gradient formulations for different values of the hygrothermal loadings $\{\widetilde{N}^T, \widetilde{N}^C\}$.

Figure 7. Static schemes: (a) cantilever nano-beam subjected to a concentrate force at the free end exposed to hygro-thermal environment; (b) simply supported nano-beam under uniformly distributed load and exposed to hygro-thermal environment.

To assess the accuracy and reliability of the proposed approach, in Tables 4 and 5, both the pure nonlocal NStrainG and NStressG dimensionless values ($\xi_1 = 0$) of the transverse displacement of the cantilever free end, $\widetilde{w}(1)$, and of the midpoint deflection, $\widetilde{w}(1/2)$, of the simply supported nano-beam, are summarized varying the nonlocal parameter, λ_c. It is worth noting that, when the hygrothermal loadings are neglected, the results obtained for $\lambda_l = 0$ coincide with those obtained in [41] and with the results presented in [53] for $\lambda_l = 0.5$.

Under the same hypothesis ($\xi_1 = 0.0$), in Tables 6 and 7, the values of the above-mentioned displacements, achieved for both $\lambda_l = 0.0$ and $\lambda_l = 0.5$, varying λ_c in the set $\{0^+, 0.1, 0.2, 0.3, 0.4, 0.5\}$ and $\{\widetilde{N}^T, \widetilde{N}^C\}$, in the set $\{(0.1, 0.01), (0.5, 0.05)\}$ are summarized. Note that, when λ_l is assumed equal to zero, the NStrainG and NStressG theories coincide with the strain-driven (EDM) and stress-driven (SDM) models, respectively.

Furthermore, the coupled effects of the nonlocal parameter, λ_c, and hygrothermal loadings $\{\widetilde{N}^T, \widetilde{N}^C\}$, on the structural response of the two nano-beams under investigation, can be derived by the graphs of Figures 8 and 9, in which the NStrainG and NStressG dimensionless displacement curves are plotted assuming $\xi_1 = 0.0$.

Table 4. Cantilever nano-beam subjected to a concentrated load at the free end: non-dimensional transverse displacement of the free end $\widetilde{\boldsymbol{w}}(\mathbf{1})$ vs. nonlocal parameter $\boldsymbol{\lambda_c}$. Comparison between nonlocal stress gradient (NStressG) and nonlocal strain gradient (NStrainG), assuming $\boldsymbol{\xi_1 = 0.0}$, $\{\widetilde{\boldsymbol{N}}^{\boldsymbol{T}}, \widetilde{\boldsymbol{N}}^{\boldsymbol{C}}\} = \{\mathbf{0.0}, \mathbf{0.0}\}$ and varying $\boldsymbol{\lambda_l}$ in the set (0.0, 0.5).

Table 5. Simply supported nano-beam under uniformly distributed load: non-dimensional midpoint deflection $\widetilde{\boldsymbol{w}}(\mathbf{1/2})$, vs. nonlocal parameter $\boldsymbol{\lambda_c}$. Comparison between nonlocal stress gradient (NStressG) and nonlocal strain gradient (NStrainG), assuming $\boldsymbol{\xi_1 = 0.0}$, $\{\widetilde{\boldsymbol{N}}^{\boldsymbol{T}}, \widetilde{\boldsymbol{N}}^{\boldsymbol{C}}\} = \{\mathbf{0.0}, \mathbf{0.0}\}$ and varying $\boldsymbol{\lambda_l}$ in the set (0.0, 0.5).

Table 6. Cantilever nano-beam subjected to a concentrated load at the free end: non-dimensional transverse displacement of the free end $\widetilde{\boldsymbol{w}}(\mathbf{1})$ vs. nonlocal parameter $\boldsymbol{\lambda_c}$. Comparison between nonlocal stress gradient (NStressG) and nonlocal strain gradient (NStrainG), assuming $\boldsymbol{\xi_1 = 0.0}$, $\{\widetilde{\boldsymbol{N}}^{\boldsymbol{T}}, \widetilde{\boldsymbol{N}}^{\boldsymbol{C}}\} = \{(\mathbf{0.1}, \mathbf{0.01}), (\mathbf{0.5}, \mathbf{0.05})\}$ and varying $\boldsymbol{\lambda_l}$ in the set (0.0, 0.5).

Table 7. Simply supported nano-beam under uniformly distributed load: non-dimensional midpoint deflection $\widetilde{\boldsymbol{w}}(\mathbf{1/2})$, vs. nonlocal parameter $\boldsymbol{\lambda_c}$. Comparison between nonlocal stress gradient (NStressG) and nonlocal strain gradient (NStrainG), assuming $\boldsymbol{\xi_1 = 0.0}$, $\{\widetilde{\boldsymbol{N}}^{\boldsymbol{T}}, \widetilde{\boldsymbol{N}}^{\boldsymbol{C}}\} = \{(\mathbf{0.1}, \mathbf{0.01}), (\mathbf{0.5}, \mathbf{0.05})\}$ and varying $\boldsymbol{\lambda_l}$ in the set (0.0, 0.5).

Figure 8. Cantilever nano-beam subjected to a concentrated load at the free end: non-dimensional transverse NStrainG and NStressG displacements, $\widetilde{\boldsymbol{w}}(\mathbf{1})$, vs. nonlocal parameter, $\boldsymbol{\lambda_c}$, assuming $\boldsymbol{\lambda_l = 0.0}$ and $\boldsymbol{\xi_1 = 0.0}$, varying $\{\widetilde{\boldsymbol{N}}^{\boldsymbol{T}}, \widetilde{\boldsymbol{N}}^{\boldsymbol{C}}\}$ in the set {(0.0, 0.0); (0.1, 0.01); (0.5, 0.05)}.

Figure 9. Simply supported nano-beam subjected to distributed load: non-dimensional transverse NStrainG and NStressG midpoint deflection, $\widetilde{\boldsymbol{w}}(\mathbf{1/2})$, vs. nonlocal parameter, $\boldsymbol{\lambda_c}$, assuming $\boldsymbol{\lambda_l = 0.0}$ and $\boldsymbol{\xi_1 = 0.0}$, varying $\{\widetilde{\boldsymbol{N}}^{\boldsymbol{T}}, \widetilde{\boldsymbol{N}}^{\boldsymbol{C}}\}$ in the set {(0.0, 0.0); (0.1, 0.01); (0.5, 0.05)}.

Moreover, the coupled effects of the mixture parameter ξ_1, the nonlocal parameter, λ_c and the dimensionless gradient length parameter λ_l on the structural responses exhibited nano-beams under investigations, are reported in the following tables and figures, varying the hygrothermal loadings:

- *Cantilever nano-beam subjected to a concentrated force at the free end*

- Figure 10, assuming $\lambda_l = 0.5$ and varying ξ_1 in the set (0.0, 0.5, 1.0) and $\{\widetilde{N}^T, \widetilde{N}^C\}$ in the set $\{(0,0); (0.1,0.01); (0.5,0.05)\}$;
- Table 8 and Figure 11a, assuming $\xi_1 = 0.0$, $\lambda_c = 0.5$, and with $\{\widetilde{N}^T, \widetilde{N}^C\}$ varying in the set $\{(0,0); (0.1,0.01); (0.5,0.05)\}$;
- Table 9 and Figure 11b, assuming $\xi_1 = 0.5$, $\lambda_c = 0.5$, and with $\{\widetilde{N}^T, \widetilde{N}^C\}$ varying in the set $\{(0,0); (0.1,0.01); (0.5,0.05)\}$;

- Table 10 and Figure 11c, assuming $\xi_1 = 1.0$, $\lambda_c = 0.5$, and with $\{\widetilde{N}^T, \widetilde{N}^C\}$ varying in the set $\{(0,0); (0.1,0.01); (0.5,0.05)\}$;

- Simply supported nano-beam subjected to a uniformly distributed load

- Figure 12, assuming $\lambda_l = 0.5$ and varying ξ_1 in the set (0.0, 0.5, 1.0) and $\{\widetilde{N}^T, \widetilde{N}^C\}$ in the set $\{(0,0); (0.1,0.01); (0.5,0.05)\}$;
- Table 11 and Figure 13a, assuming $\xi_1 = 0.0$, $\lambda_c = 0.5$, and with $\{\widetilde{N}^T, \widetilde{N}^C\}$ varying in the set $\{(0,0); (0.1,0.01); (0.5,0.05)\}$;
- Table 12 and Figure 13b, assuming $\xi_1 = 0.5$, $\lambda_c = 0.5$, and with $\{\widetilde{N}^T, \widetilde{N}^C\}$ varying in the set $\{(0,0); (0.1,0.01); (0.5,0.05)\}$;
- Table 13 and Figure 13c, assuming $\xi_1 = 1.0$, $\lambda_c = 0.5$, and with $\{\widetilde{N}^T, \widetilde{N}^C\}$ varying in the set $\{(0,0); (0.1,0.01); (0.5,0.05)\}$.

From the numerical evidence of Tables 4-13 and the corresponding curves plotted in Figures 8-13, it is interesting to underline that local/nonlocal stress-driven and strain-driven gradient theories are able to simulate both a softening and stiffening size-dependent structural response of inflected nano-beams with internal uniform porosity under hygro-thermo-mechanical loadings. A softening response is exhibited by NStrainG formulation when increasing the nonlocal parameter, λ_c, (see Figures 10 and 12) and a stiffening behavior is observed when increasing the gradient length parameter, λ_l (see Figures 11 and 13) and the mixture parameter ξ_1 (see Tables 8-10 and Tables 11-13).

On the contrary, a stiffening response is exhibited by NStressG theory when increasing the nonlocal parameter, λ_c (see Figures 10 and Figures 12) and a softening behavior is observed when increasing the gradient length parameter, λ_l (see Figures 11 and 13) and the mixture parameter ξ_1 (see Tables 8-10 and Tables 11-13).

In addition, the numerical results demonstrate that the increase in the temperature and moisture concentrations, here simulated in terms of the hygro-thermal axial force resultants, $\widetilde{N}^T$ and $\widetilde{N}^C$, leads to an increase in the bending behavior for both the cantilever and simply supported nano-beams.

Figures 10(a-c). Cantilever nano-beam subjected to a concentrated load at the free end: non-dimensional transverse NStrainG and NStressG displacements, $\widetilde{\boldsymbol{w}}(\mathbf{1})$, vs. nonlocal parameter, $\boldsymbol{\lambda_c}$, assuming $\boldsymbol{\lambda_l = 0.5}$, and $\boldsymbol{\xi_1 = 0.0}$ (a), $\boldsymbol{\xi_1 = 0.5}$ (b), $\boldsymbol{\xi_1 = 1.0}$ (c), and varying $\{\widetilde{\boldsymbol{N}}^{\boldsymbol{T}}, \widetilde{\boldsymbol{N}}^{\boldsymbol{C}}\}$ in the set {(0.0, 0.0); (0.1, 0.01); (0.5, 0.05)}.

Figures 11(a-c). Cantilever nano-beam subjected to a concentrated load at the free end: non-dimensional transverse NStrainG and NStressG displacements, $\widetilde{\boldsymbol{w}}(\mathbf{1})$, vs. gradient length parameter, $\boldsymbol{\lambda_l}$, assuming $\boldsymbol{\lambda_c = 0.5}$ and $\boldsymbol{\xi_1 = 0.0}$ (a), $\boldsymbol{\xi_1 = 0.5}$ (b), $\boldsymbol{\xi_1 = 1.0}$ (c), and varying $\{\widetilde{\boldsymbol{N}}^{\boldsymbol{T}}, \widetilde{\boldsymbol{N}}^{\boldsymbol{C}}\}$ in the set {(0.0, 0.0); (0.1, 0.01); (0.5, 0.05)}.

Table 8. Cantilever nano-beam subjected to a concentrated load at the free end: non-dimensional transverse displacement of the free end $\widetilde{\boldsymbol{w}}(\mathbf{1})$ vs. gradient length parameter $\boldsymbol{\lambda_l}$, with the nonlocal parameter $\boldsymbol{\lambda_c = 0.5}$, evaluated by $\boldsymbol{\xi_1 = 0.0}$ in NStrainG and NStressG varying $\{\widetilde{\boldsymbol{N}}^{\boldsymbol{T}}, \widetilde{\boldsymbol{N}}^{\boldsymbol{C}}\}$ in the set {(0.0, 0.0); (0.1, 0.01); (0.5, 0.05)}.

Table 9. Cantilever nano-beam subjected to a concentrated load at the free end: non-dimensional transverse displacement of the free end $\widetilde{\boldsymbol{w}}(\mathbf{1})$ vs. gradient length parameter $\boldsymbol{\lambda_l}$, with the nonlocal parameter $\boldsymbol{\lambda_c = 0.5}$, evaluated by $\boldsymbol{\xi_1 = 0.5}$ in NStrainG and NStressG varying $\{\widetilde{\boldsymbol{N}}^{\boldsymbol{T}}, \widetilde{\boldsymbol{N}}^{\boldsymbol{C}}\}$ in the set {(0.0, 0.0); (0.1, 0.01); (0.5, 0.05)}.

Table 10. Cantilever nano-beam subjected to a concentrated load at the free end: non-dimensional transverse displacement of the free end $\widetilde{\boldsymbol{w}}(\mathbf{1})$ vs. gradient length parameter $\boldsymbol{\lambda_l}$, with the nonlocal parameter $\boldsymbol{\lambda_c = 0.5}$, evaluated by $\boldsymbol{\xi_1 = 1.0}$ in NStrainG and NStressG varying $\{\widetilde{\boldsymbol{N}}^{\boldsymbol{T}}, \widetilde{\boldsymbol{N}}^{\boldsymbol{C}}\}$ in the set {(0.0, 0.0); (0.1, 0.01); (0.5, 0.05)}.

Figures 12(a-c). Simply supported nano-beam under a uniformly distributed load: non-dimensional midpoint deflection $\widetilde{\boldsymbol{w}}(\mathbf{1/2})$ vs. nonlocal parameter $\boldsymbol{\lambda_c}$, with the gradient length parameter $\boldsymbol{\lambda_l = 0.5}$, evaluated by $\boldsymbol{\xi_1 = 0.0}$ (a), $\boldsymbol{\xi_1 = 0.5}$ (b) and $\boldsymbol{\xi_1 = 1.0}$ (c) in NStrainG and NStressG varying $\{\widetilde{\boldsymbol{N}}^{\boldsymbol{T}}, \widetilde{\boldsymbol{N}}^{\boldsymbol{C}}\}$ in the set {(0.0, 0.0); (0.1, 0.01); (0.5, 0.05)}.

Figures 13(a-c). Simply supported nano-beam under a uniformly distributed load: non-dimensional midpoint deflection $\widetilde{\boldsymbol{w}}(\mathbf{1/2})$ vs. gradient length parameter $\boldsymbol{\lambda_l}$, with the nonlocal parameter $\boldsymbol{\lambda_c = 0.5}$, evaluated by $\boldsymbol{\xi_1 = 0.0}$ (a), $\boldsymbol{\xi_1 = 0.5}$ (b) and $\boldsymbol{\xi_1 = 1.0}$ (c) in NStrainG and NStressG varying $\{\widetilde{\boldsymbol{N}}^{\boldsymbol{T}}, \widetilde{\boldsymbol{N}}^{\boldsymbol{C}}\}$ in the set {(0.0, 0.0); (0.1, 0.01); (0.5, 0.05)}.

Table 11. Simply supported nano-beam under uniformly distributed: non-dimensional midpoint deflection $\widetilde{\boldsymbol{w}}(\mathbf{1/2})$ vs. gradient length parameter $\boldsymbol{\lambda_l}$, with the nonlocal parameter $\boldsymbol{\lambda_c = 0.5}$, evaluated by $\boldsymbol{\xi_1 = 0.0}$ in NStrainG and NStressG varying $\{\widetilde{\boldsymbol{N}}^{\boldsymbol{T}}, \widetilde{\boldsymbol{N}}^{\boldsymbol{C}}\}$ in the set {(0.0, 0.0); (0.1, 0.01); (0.5, 0.05)}.

Table 12. Simply supported nano-beam under uniformly distributed: non-dimensional midpoint deflection $\widetilde{\boldsymbol{w}}(\mathbf{1/2})$ vs. gradient length parameter $\boldsymbol{\lambda_l}$, with the nonlocal parameter $\boldsymbol{\lambda_c = 0.5}$, evaluated by $\boldsymbol{\xi_1 = 0.5}$ in NStrainG and NStressG varying $\{\widetilde{\boldsymbol{N}}^{\boldsymbol{T}}, \widetilde{\boldsymbol{N}}^{\boldsymbol{C}}\}$ in the set {(0.0, 0.0); (0.1, 0.01); (0.5, 0.05)}.

Table 13. Simply supported nano-beam under uniformly distributed: non-dimensional midpoint deflection $\widetilde{\boldsymbol{w}}(\mathbf{1/2})$ vs. gradient length parameter $\boldsymbol{\lambda_l}$, with the nonlocal parameter $\boldsymbol{\lambda_c = 0.5}$, evaluated by $\boldsymbol{\xi_1 = 1.0}$ in NStrainG and NStressG varying $\{\widetilde{\boldsymbol{N}}^{\boldsymbol{T}}, \widetilde{\boldsymbol{N}}^{\boldsymbol{C}}\}$ in the set {(0.0, 0.0); (0.1, 0.01); (0.5, 0.05)}.

6. Conclusions

This paper considered the bending response of a porous FG Euler-Bernoulli nano-beam subjected to hygro-thermo-mechanical loadings using both local/nonlocal stress-driven and strain-driven gradient formulations. The governing equations were derived by using the virtual work principle. A Wolfram language code in Mathematica was then written to carry out a parametric investigation for different boundary conditions including cantilever and simply-supported conditions.

Firstly, the effects of some parameters, such as porosity volume fraction, the gradient index, moisture concentration and hygro-thermal changes on the elastic characteristics of a porous functionally graded material, were investigated. Moreover, a parametric investigation on the structural bending behavior of FG porous nano-beams varying the nonlocal parameter, the gradient length parameter, the hygro-thermo-mechanical loadings and the mixture parameter of both local/nonlocal strain (NStrainG) and stress gradient (NStressG) formulations was presented.

From the above investigation, we can draw some conclusions as follows:

- increasing the porosity, the gradient index and the thermal rise reduces the bending and axial stiffnesses of the FG nano-beam with it generally leading to an increase in bending flexibility;
- a softening response has been exhibited by NStrainG formulation when increasing the nonlocal parameter and a stiffening behavior is observed when increasing the gradient length parameter and the mixture parameter;
- a stiffening response is exhibited by NStressG theory when increasing the nonlocal parameter and a softening behavior is observed when increasing the gradient length parameter and the mixture parameter;
- upon increasing the temperature and moisture concentrations leads to an increase in the bending deflection of the nano-beams related to a decrease in the bending stiffness due to an abatement of the thermo-elastic properties of the porous FG material.

In conclusion, the proposed approach represents a cost-effective method to capture the bending behavior of inflected porous functionally graded Bernoulli–Euler nano-beams subjected to severe environmental conditions.

References

1. Jha DK, Kant T, Singh RK. A critical review of recent research on functionally graded plates. Compos Struct 2013; 96:833–49.
2. Su Z, Jin G, Ye T. Three-dimensional vibration analysis of thick functionally graded conical, cylindrical shell and annular plate structures with arbitrary elastic restraints. Compos Struct 2014;118: 432–47.
3. Bassiouny S, Jinghua J, Reham F, Tareq A, Qiong X, Lisha W, Dan S, Aibin M. 30 Years of functionally graded materials: An overview of manufacturing methods, Applications and Future Challenges. Compos. B 2020; 201:108376.
4. Kumar R, Singh R, Hui D, Feo L, Fraternali F. Graphene as biomedical sensing element: State of art review and potential engineering applications. Compos B 2018; 134:193–206.
5. Zhou XW, Dai HL, Wang L. Dynamics of axially functionally graded cantilevered pipes conveying fluid. Compos Struct 2018; 190:112–8.
6. Barati MR and Shahverdi H. A four-variable plate theory for thermal vibration of embedded FG nanoplates under non-uniform temperature distributions with different boundary conditions. Struct. Eng. Mech., Int. J. 2016; 60(4):707-727.
7. Kar VR and Panda SK. Nonlinear flexural vibration of shear deformable functionally graded spherical shell panel. Steel Compos. Struct. Int. J. 2055; 18(3):693-709.
8. Houari MSA, Tounsi A, Bessaim A. and Mahmoud SR. A new simple three-unknown sinusoidal shear deformation theory for functionally graded plates. Steel Compos. Struct., Int. J. 2016; 22(2):257-276.
9. Tlidji, Y, Zidour M, Draiche K, Safa A., Bourada M., Tounsi A, Bousahla AA. and Mahmoud SR. Vibration analysis of different material distributions of functionally graded microbeam. Struct. Eng. Mech., Int. J. 2019; 69(6):637-649.
10. Sekkal M, Fahsi B, Tounsi A. and Mahmoud SR. A novel and simple higher order shear deformation theory for stability and vibration of functionally graded sandwich plate. Steel Compos. Struct. Int. J. 2017; 25(4):389-401.
11. Karami B, Shahsavari D, Janghorban M and Tounsi A. Resonance behavior of functionally graded polymer composite nanoplates reinforced with grapheme nanoplatelets. Int. J. Mech. Sci. 2019; 156:94-105.
12. García-Macías E, D'Alessandro A, Castro-Triguero R, Pérez-Mira D, Ubertini F. Micromechanics modeling of the uniaxial strain-sensing property ofcarbon nanotube cement-matrix composites for SHM applications. Compos. Struct. 2017; 163:195-215.
13. Cortes H, Pfeiffer C, Richter B, Stevens T. Porous ceramic bed supports for fused silica packed capillary columns used in liquid chromatography. J. Sep. Sci 1987;10(8):446-448.
14. Krespe C, Leonowicz M, Roth WJ, Vartuli J, Beck J. Ordered mesoporous molecular sieves synthesized by a liquid-crystal template mechanism. Nature 1992; 357:(6397)710.
15. Beck J, Vartuli J, Roth WJ, Leonowicz M, Kresge C, Schmitt K, Chu C, Olson DH, Sheppard E, McCullen S, et al. A new family of mesoporous molecular sieves prepared with liquid crystal templates. J. Am. Chem. Soc. 1992; 114 (27):10834-10843.
16. Velev O, Jede T, Lobo R, Lenhoff A. Porous silica via colloidal crystallization. Nature 389 1997; 6650:447.
17. Lefebvre LP, Banhart J, Dunand DC. Porous metals and metallic foams: current status and recent developments. Adv. Eng. Mater 2008; 10(9):775-787.
18. Zhao C. Review on thermal transport in high porosity cellular metal foams with open cells. Int. J. Heat Mass Transf. 2012; 55(13):3618-3632.
19. Acierno S, Barretta R, Luciano R, Marotti de Sciarra F, Russo P. Experimental evaluations and modeling of the tensile behavior of polypropylene/single-walled carbon nanotubes fibers. Composite Structures 2017;174:12–18.
20. Aifantis EC, Internal length gradient (ILG) material mechanics across scales and disciplines. Adv Appl Mech 2016; 49:1–110. https://doi.org/10.1016/bs.aams. 2016.08.00.
21. Eringen AC. Linear theory of nonlocal elasticity and dispersion of plane waves. Int J Eng Sci 1972; 10(5):425-35.
22. Eringen AC. On differential equations of nonlocal elasticity and solutions of screw dislocation and surface waves. J Appl Phys 1983; 54:4703–10.
23. Lim CW, Zhang G, and Reddy JN. A higher-order nonlocal elasticity and strain gradient theory and its applications in wave propagation. J. Mech. Phys. Solids 2015;78:298–313.
24. Mindlin RD. Micro-structure in linear elasticity. Arch Ration Mech Anal 1964; 16:51–78.

25. Mindlin RD. Second gradient of strain and surface-tension in linear elasticity. Int. J. Solids Struct.1 1965;417–438. https://doi.org/10.1016/0020-7683(65)90006-5.
26. Tanga Y, Ding Q. Nonlinear vibration analysis of a bi-directional functionally graded beam under hygro-thermal loads. Compos Struct. 2019;225,111076.
27. Lee CY, Kim JH. Hygrothermal postbuckling behavior of functionally graded plates. Compos Struct 2013;95:278–82.
28. Shen HS. Nonlinear analysis of functionally graded fiber reinforced composite laminated beams in hygrothermal environments, Part I: Theory and solutions. Compos Struct 2015;125:698–705.
29. Shen HS. Nonlinear analysis of functionally graded fiber reinforced composite laminated beams in hygrothermal environments, Part II: numerical results. Compos Struct 2015;125:706–12.
30. Nguyen TK, Nguyen BD, Vo TP, Thai HT. Hygro-thermal effects on vibration and thermal buckling behaviours of functionally graded beams. Compos Struct 2017;176:1050–60.
31. Bouazza M, Zenkour AM. Hygro-thermo-mechanical buckling of laminated beam using hyperbolic refined shear deformation theory. Compos Struct 2020;252:112689.
32. Jouneghanim FZ, Dimitri R, Tornabene F. Structural response of porous FG nanobeams under hygro-thermo-mechanical loadings. Compos. B 2017;152:71-78.
33. Dastjerdi S, Malikan M, Dimitri R, Tornabene F. Nonlocal elasticity analysis of moderately thick porous functionally graded plates in a hygro-thermal environment. Compos Struct 2021;255: 112925.
34. Ebrahimi F, Barati MR. Unified formulation for dynamic analysis of nonlocal heterogeneous nanobeams in hygro-thermal environment. Appl. Phys. A 122 2016;792.
35. Ebrahimi F, Barati MR. Small-scale effects on hygro-thermo-mechanical vibration of temperature-dependent nonhomogeneous nanoscale beams. Mech Adv Mater Struct 2017;24(11):924–36.
36. Ebrahimi F, Barati MR. Hygrothermal effects on vibration characteristics of viscoelastic FG nanobeams based on nonlocal strain gradient theory. Compos. Struct. 2017;159:433–444.
37. Chu L, Dui G, Zheng Y. Thermally induced nonlinear dynamic analysis of temperature-dependent functionally graded flexoelectric nanobeams based on nonlocal simplified strain gradient elasticity theory. European Journal of Mechanics/A Solids 2020;82:103999.
38. Romano G, Barretta R, Diaco M, Marotti de Sciarra F. Constitutive boundary conditions and paradoxes in nonlocal elastic nano-beams. Int J Mech Sci 2017;121:151-6.
39. Romano G, Barretta R. Nonlocal elasticity in nanobeams: The stress-driven integral model. International Journal of Engineering Science 2017; 115:14–27 .
40. Barretta R, Fazelzadeh SA, Feo L, Ghavanloo E, Luciano R. Nonlocal inflected nano-beams: A stress-driven approach of bi-Helmholtz type. Compos. Struct. 2018;200:239–45.
41. Barretta R, Canadija M, Feo L, Luciano R, Marotti de Sciarra F, Penna R. Exact solutions of inflected functionally graded nano-beams in integral elasticity. Compos. B 2018; 142:273–86.
42. Barretta R, Luciano R, Marotti de Sciarra F, Ruta G. Stress-driven nonlocal integral model for Timoshenko elastic nano-beams. European Journal of Mechanics - A/Solids 2018; 72:275-28.
43. Barretta R, Diaco M, Feo L, Luciano R, Marotti de Sciarra F, Penna R. Stress-driven integral elastic theory for torsion of nano-beams. Mechanics Research Communications 2018; 87:35–41.
44. Barretta R, Canadija M, Luciano R, Marotti de Sciarra F. Stress-driven modeling of nonlocal thermoelastic behavior of nanobeams. International Journal of Engineering Science 2018; 126:53–67.
45. Barretta R, Fabbrocino F, Luciano R, Marotti de Sciarra F. Closed-form solutions in stress-driven two-phase integral elasticity for bending of functionally graded nano-beams. Physica E 2018; 97:13–30.
46. Barretta R, Faghidian SA, Luciano R, Medaglia CM, Penna R. Stress-driven two-phase integral elasticity for torsion of nano-beams. Compos.B 2018;145:62–69.
47. Barretta R, Faghidian SA, Luciano R. Longitudinal vibrations of nanorods by stress driven integral elasticity. Mechanics of Advanced Materials and Structures 2018;26:1307-1315.
48. Darban H, Fabbrocino F, Feo L, Luciano R. Size-dependent buckling analysis of nanobeams resting on two-parameter elastic foundation through stress-driven nonlocal elasticity model. Mechanics of Advanced Materials and Structures, Mechanics of Advanced Materials and Structures 2020;1-9.
49. Apuzzo A, Barretta R, Luciano R, Marotti de Sciarra F, Penna R. Free vibrations of Bernoulli–Euler nano-beams by the stress-driven nonlocal integral model. Compos. B 2017;123:105–111.
50. Penna R, Feo L, Fortunato A, Luciano R. Nonlinear free vibrations analysis of geometrically imperfect FG nano-beams based on stress-driven nonlocal elasticity with initial pretension force. Compos. Struct. 2021; 255:112856.
51. Penna R, Feo L. Nonlinear Dynamic Behavior of Porous and Imperfect Bernoulli-Euler Functionally Graded Nanobeams Resting on Winkler Elastic Foundation. *Technologies* 2020;8:56.

52. Zaera R, Serrano Ó, Fernández-Sáez R. On the consistency of the nonlocal strain gradient elasticity. International Journal of Engineering Science 2019;138:65–81.
53. Barretta R, Marotti de Sciarra F. Variational nonlocal gradient elasticity for nano-beams. International Journal of Engineering Science 2019; 143:73–91.
54. Pinnola FP, Faghidian SA Barretta R, Marotti de Sciarra F. Variationally consistent dynamics of nonlocal gradient elastic beams. International Journal of Engineering Science 2020;149:103220.

Hygro-thermal bending behavior of porous FG nano-beams via local/nonlocal strain and stress gradient theories of elasticity

Rosa PENNA, Luciano FEO, Giuseppe LOVISI

Department of Civil Engineering, University of Salerno, 84084, Fisciano, Italy

FIGURES

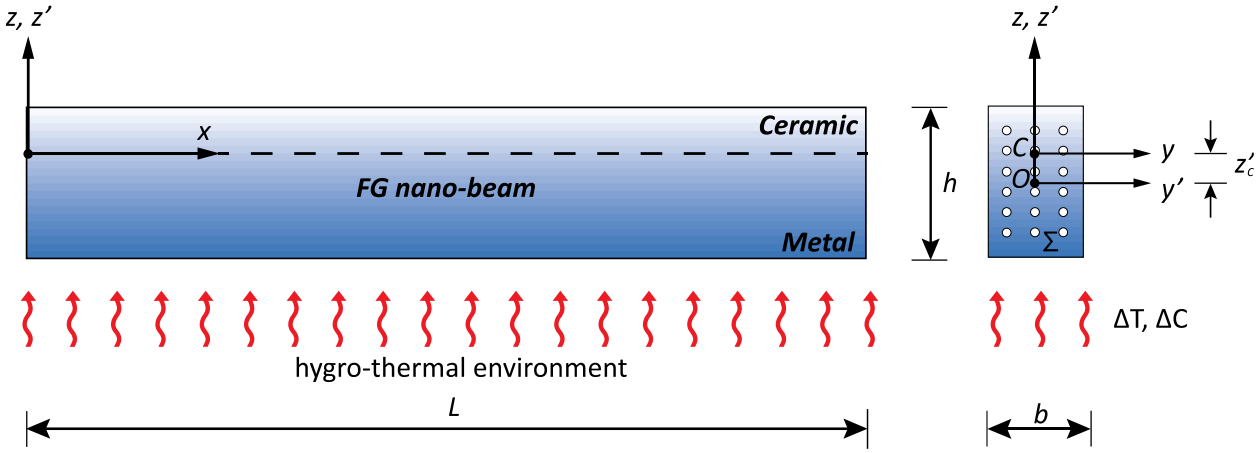

Figure 1. Coordinate system and configuration of a porous FG Bernoulli-Euler nano-beam.

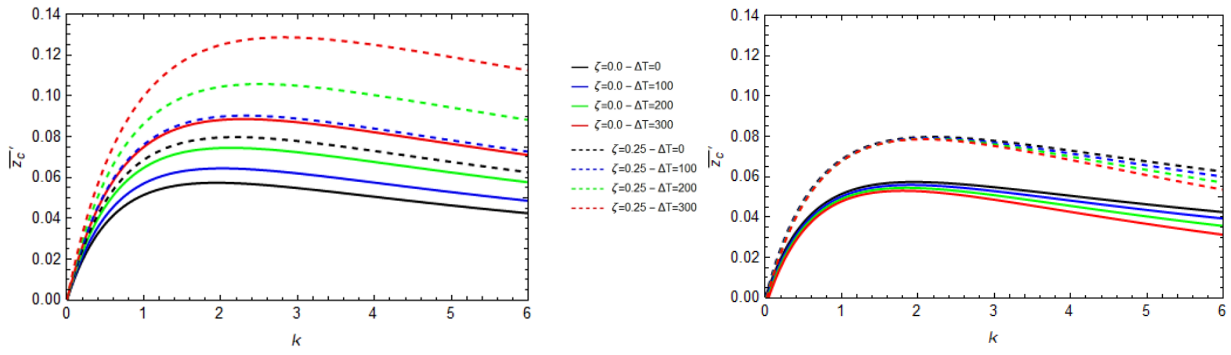

(a) uniform temperature rise

(b) linear temperature rise

Figures 2. Effects of the gradient index (k) on the dimensionless position of the elastic centre C for non-porous ($\zeta = 0.0$) and porous ($\zeta = 0.25$) FG materials under uniform (a) and linear (b) temperature rises (ΔT=0, 100, 200, 300 [K]).

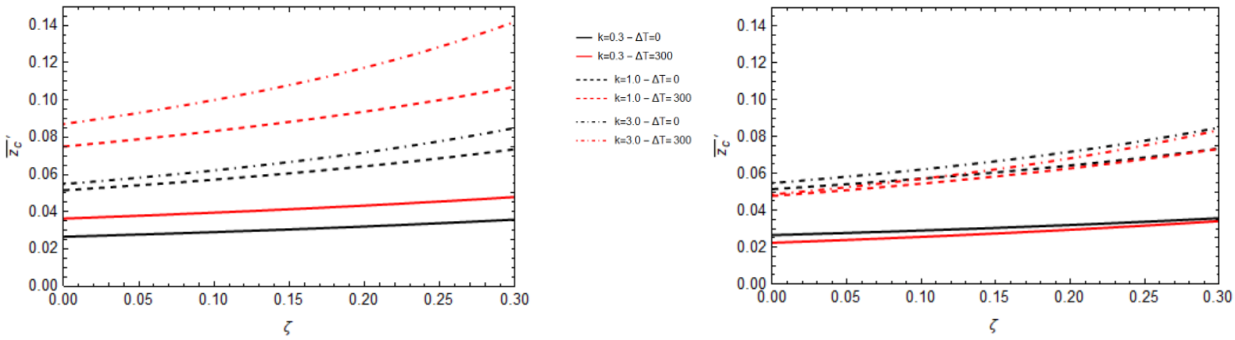

(a) uniform temperature rise

(b) linear temperature rise

Figures 3. Effects of the porosity volume fraction (ζ) on the dimensionless position of the elastic centre *C* for three different values of the material gradient index (*k=0.3,1.0,3.0*) under uniform (a) and linear (b) temperature rises (ΔT=0, 300 [K]).

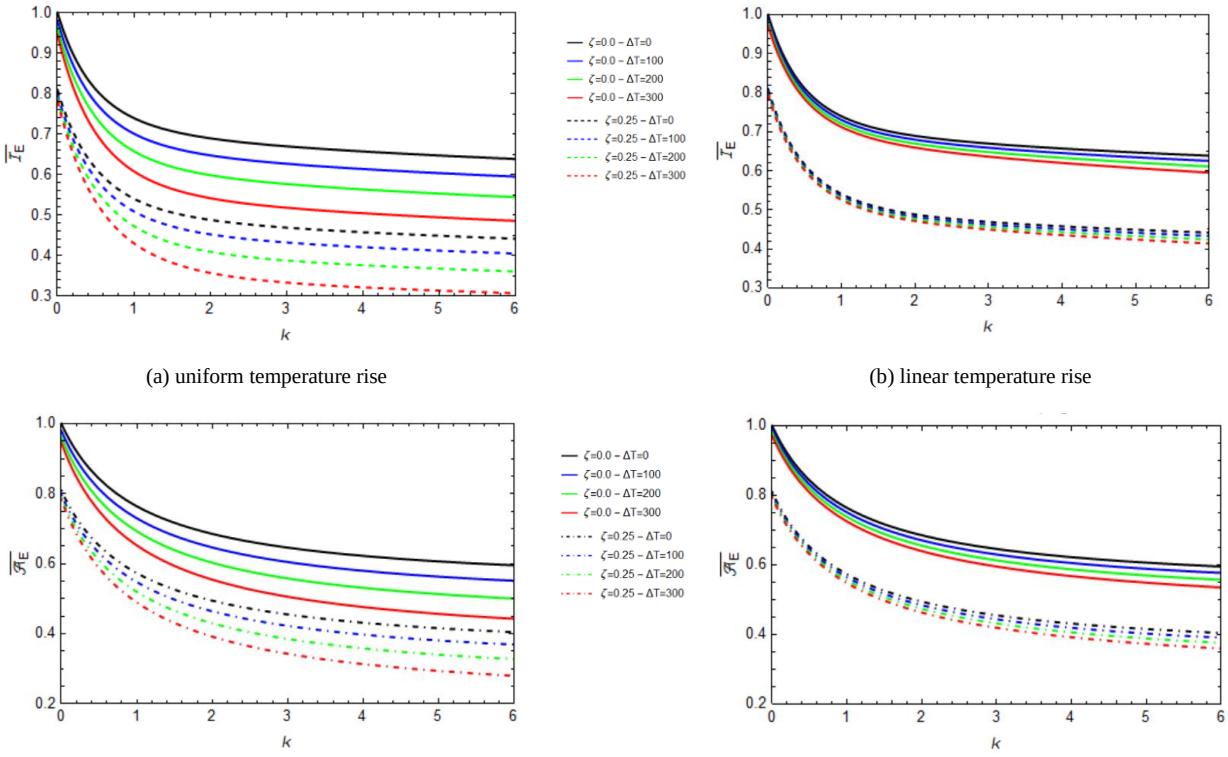

(a) uniform temperature rise

(b) linear temperature rise

(c) uniform temperature rise

(d) linear temperature rise

Figures 4. Effects of the gradient index (k) on the dimensionless bending stiffness $\overline{I_E}$ (a,b) and axial stiffness $\overline{A_E}$ (c,d) for non-porous ($\zeta = 0.0$) and porous ($\zeta = 0.25$) FG materials under uniform (a,c) and linear (b,d) temperature rises (ΔT=0, 100, 200, 300 [K]).

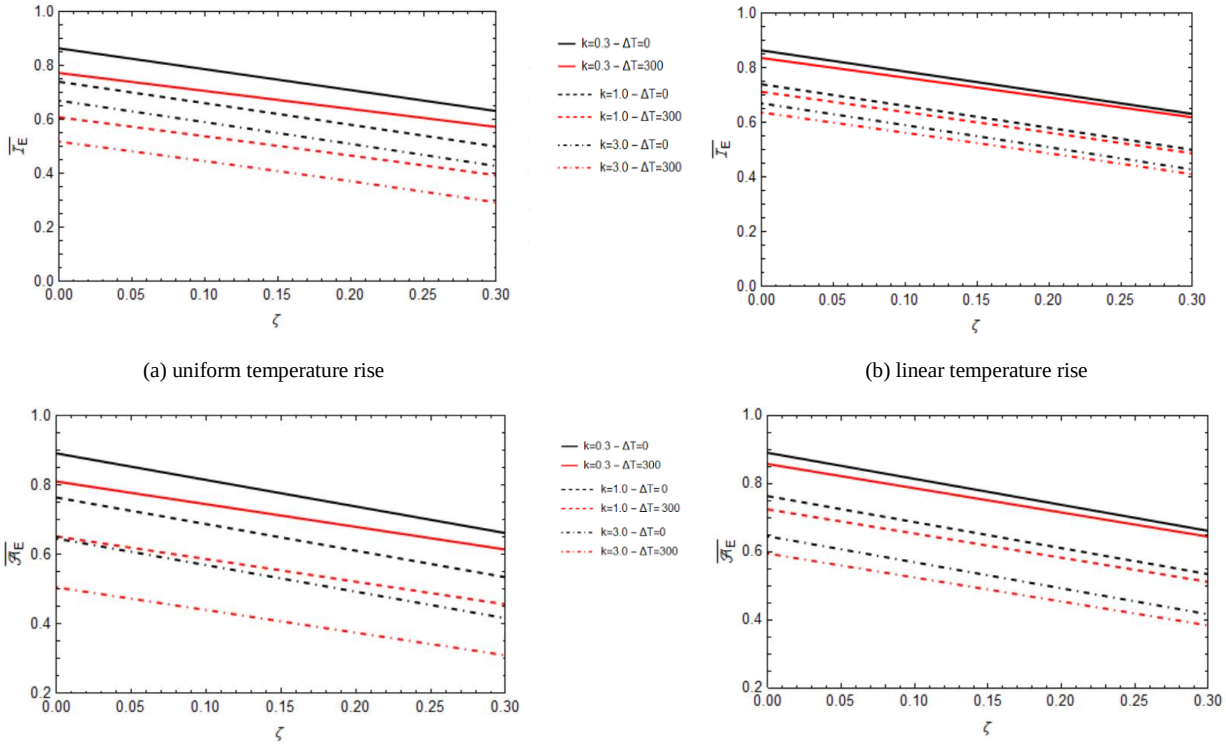

(a) uniform temperature rise

(b) linear temperature rise

(c) uniform temperature rise

(d) linear temperature rise

Figures 5. Effects of the porosity volume fraction (ζ) on the dimensionless bending stiffness $\overline{I_E}$ (a,b) and axial stiffness $\overline{A_E}$ (c,d) for three different values of the gradient index (*k=0.3,1.0,3.0*) of the FG material under uniform (a,c) and linear (b,d) temperature rises (ΔT=0, 300 [K]).

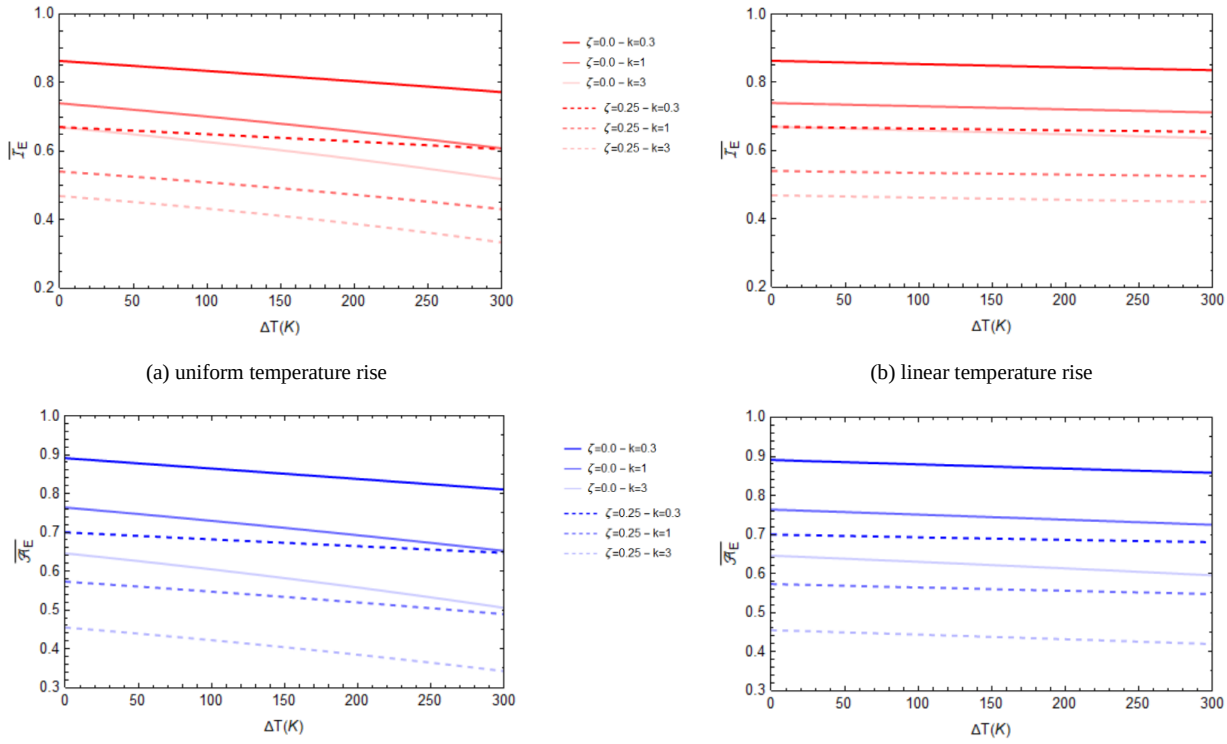

(a) uniform temperature rise

(b) linear temperature rise

(c) uniform temperature rise

(d) linear temperature rise

Figures 6. Effects of uniform (a,c) and linear (b,d) temperature rises on the dimensionless bending stiffness $\overline{I_E}$ (a, b) and axial stiffness $\overline{A_E}$ (c, d) for non-porous ($\zeta = 0.0$) and porous ($\zeta = 0.25$) FG materials and for three different values of the gradient index (*k=0.3,1.0,3.0*).

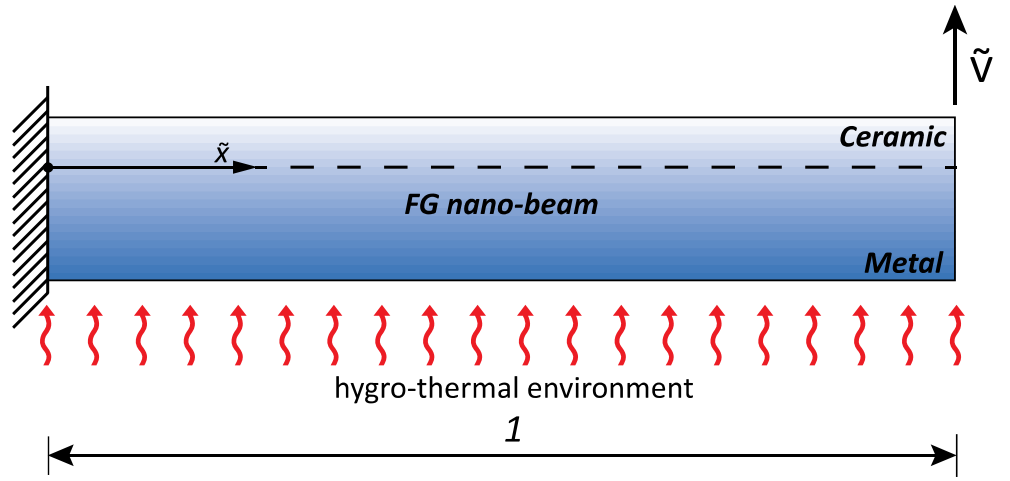

(a)

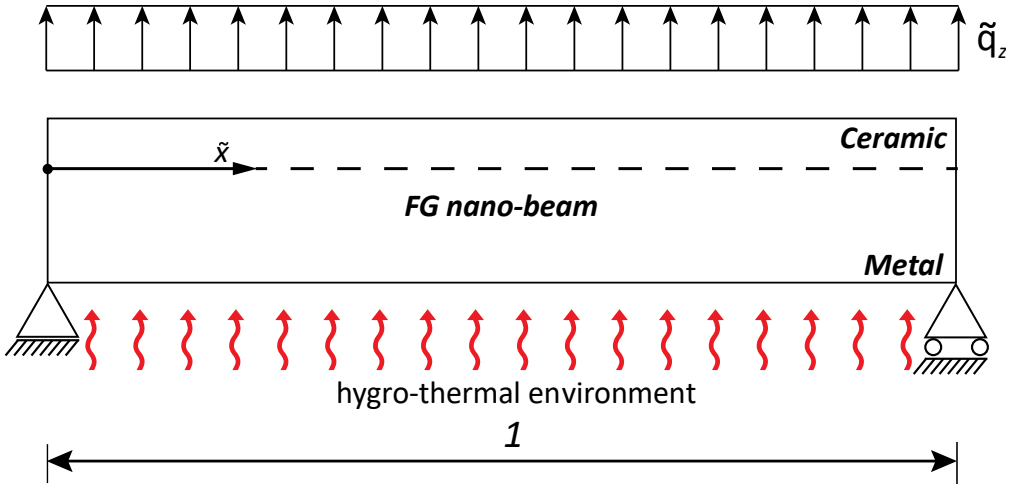

(b)

Figure 7. Static schemes: (a) cantilever nano-beam subjected to a concentrate force at the free end exposed to hygro-thermal environment; (b) simply supported nano-beam under uniformly distributed load and exposed to hygro-thermal environment.

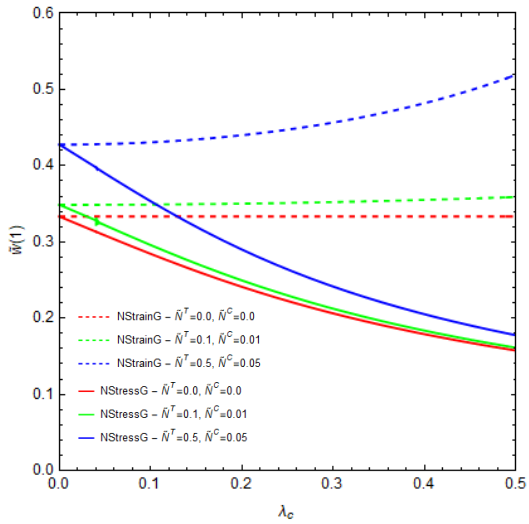

Figure 8. Cantilever nano-beam subjected to a concentrated load at the free end: non-dimensional transverse NStrainG and NStressG displacements, $\tilde{\boldsymbol{w}}(\mathbf{1})$, vs. nonlocal parameter, $\boldsymbol{\lambda_c}$, assuming $\boldsymbol{\lambda_l = 0.0}$ and $\boldsymbol{\xi_1 = 0.0}$, varying $\{\tilde{\boldsymbol{N}}^{\boldsymbol{T}}, \tilde{\boldsymbol{N}}^{\boldsymbol{C}}\}$ in the set {(0.0, 0.0); (0.1, 0.01); (0.5, 0.05)}.

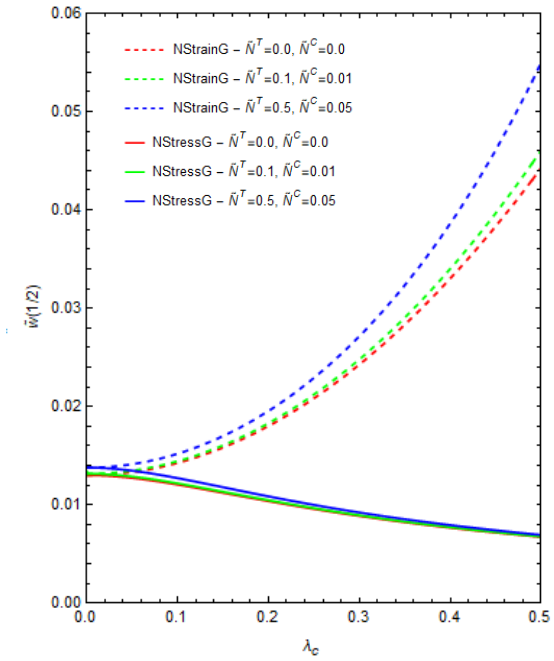

Figure 9. Simply supported nano-beam subjected to a distributed load: non-dimensional transverse NStrainG and NStressG midpoint deflection, $\tilde{\boldsymbol{w}}(\mathbf{1/2})$, vs. nonlocal parameter, $\boldsymbol{\lambda_c}$, assuming $\boldsymbol{\lambda_l = 0.0}$ and $\boldsymbol{\xi_1 = 0.0}$, varying $\{\tilde{\boldsymbol{N}}^{\boldsymbol{T}}, \tilde{\boldsymbol{N}}^{\boldsymbol{C}}\}$ in the set {(0.0, 0.0); (0.1, 0.01); (0.5, 0.05)}.

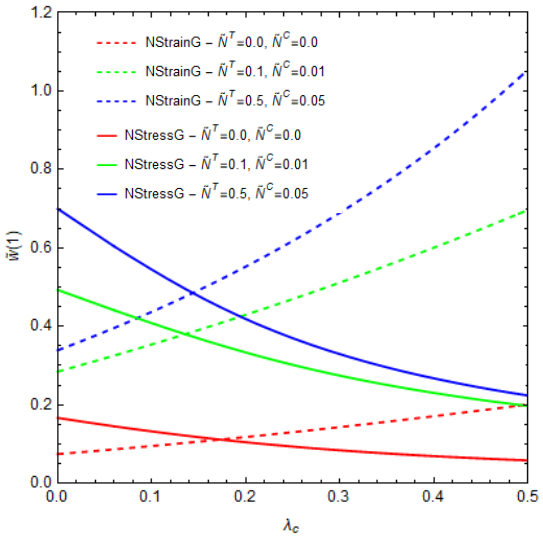

(**a**)

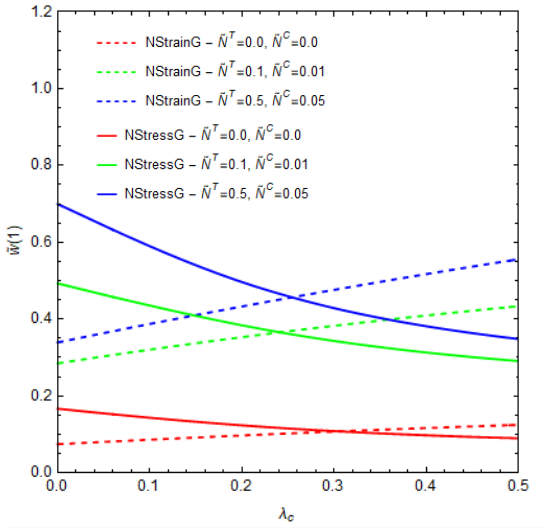

(**b**)

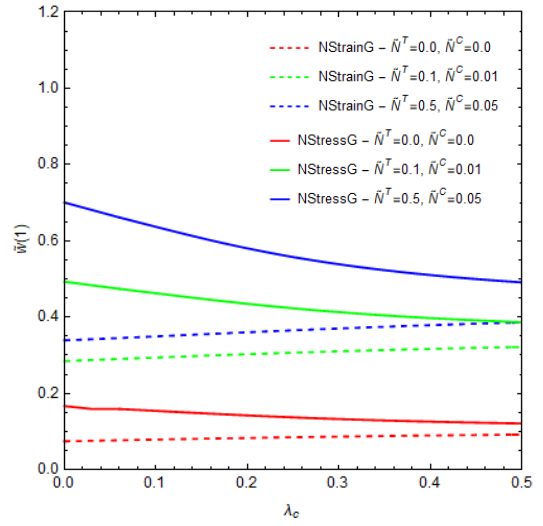

(**c**)

Figures 10(a-c). Cantilever nano-beam subjected to a concentrated load at the free end: non-dimensional transverse NStrainG and NStressG displacements, $\widetilde{\boldsymbol{w}}(\mathbf{1})$, vs. nonlocal parameter, $\boldsymbol{\lambda_c}$, assuming $\boldsymbol{\lambda_l = 0.5}$, and $\boldsymbol{\xi_1 = 0.0}$ (a), $\boldsymbol{\xi_1 = 0.5}$ (b), $\boldsymbol{\xi_1 = 1.0}$ (c), and varying $\{\widetilde{\boldsymbol{N}}^{\boldsymbol{T}}, \widetilde{\boldsymbol{N}}^{\boldsymbol{C}}\}$ in the set {(0.0, 0.0); (0.1, 0.01); (0.5, 0.05)}.

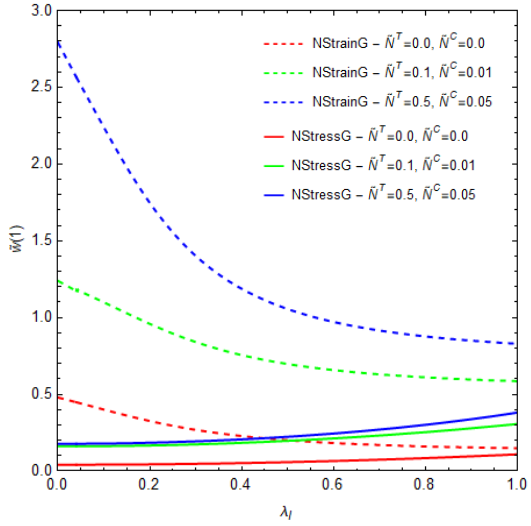

(**a**)

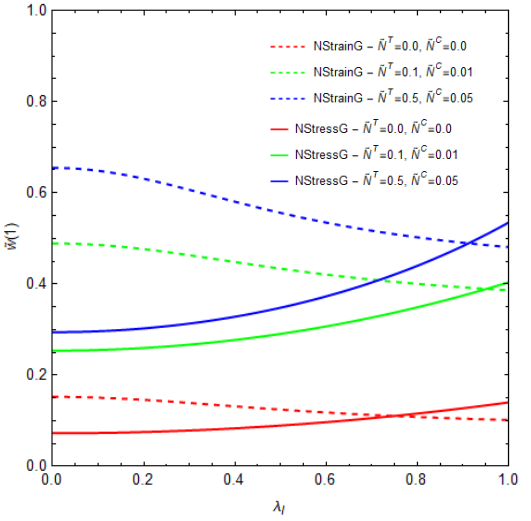

(**b**)

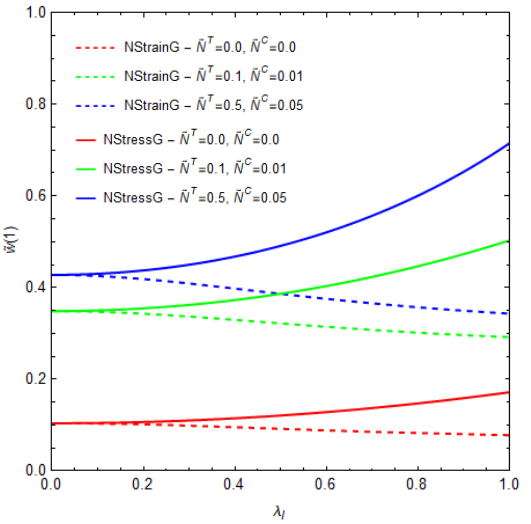

(**c**)

Figures 11(a-c). Cantilever nano-beam subjected to a concentrated load at the free end: non-dimensional transverse NStrainG and NStressG displacements, $\widetilde{\boldsymbol{w}}(\mathbf{1})$, vs. gradient length parameter, $\boldsymbol{\lambda_l}$, assuming $\boldsymbol{\lambda_c = 0.5}$ and $\boldsymbol{\xi_1 = 0.0}$ (a), $\boldsymbol{\xi_1 = 0.5}$ (b), $\boldsymbol{\xi_1 = 1.0}$ (c), and varying $\{\widetilde{\boldsymbol{N}}^{\boldsymbol{T}}, \widetilde{\boldsymbol{N}}^{\boldsymbol{C}}\}$ in the set {(0.0, 0.0); (0.1, 0.01); (0.5, 0.05)}.

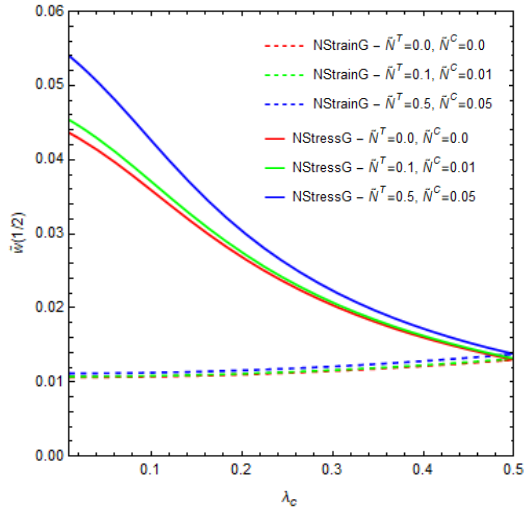

(**a**)

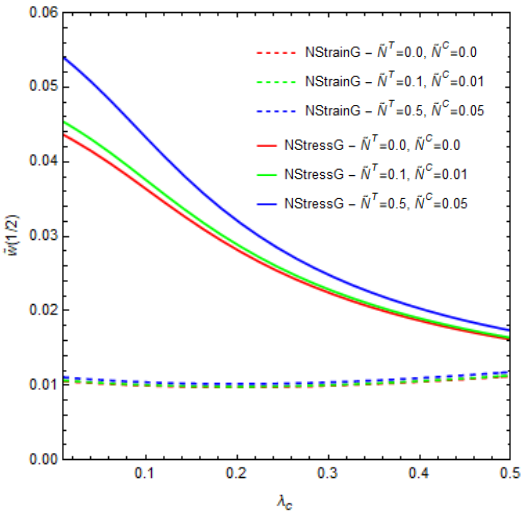

(**b**)

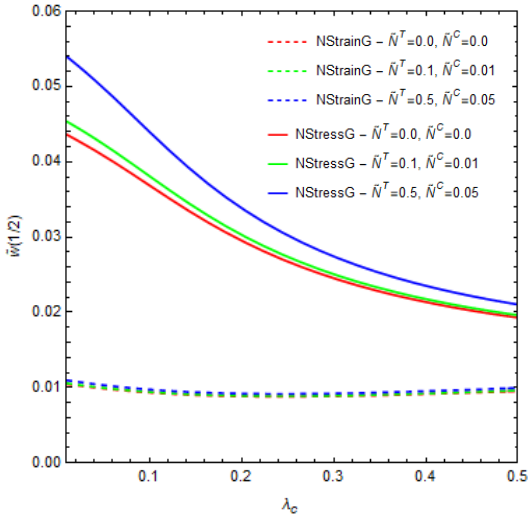

(**c**)

Figures 12(a-c). Simply supported nano-beam under a uniformly distributed load: non-dimensional midpoint deflection $\widetilde{\boldsymbol{w}}(\mathbf{1/2})$ vs. nonlocal parameter $\boldsymbol{\lambda_c}$, with the gradient length parameter $\boldsymbol{\lambda_l = 0.5}$, evaluated by $\boldsymbol{\xi_1 = 0.0}$ (a), $\boldsymbol{\xi_1 = 0.5}$ (b) and $\boldsymbol{\xi_1 = 1.0}$ (c) in NStrainG and NStressG varying $\{\widetilde{\boldsymbol{N}}^{\boldsymbol{T}}, \widetilde{\boldsymbol{N}}^{\boldsymbol{C}}\}$ in the set {(0.0, 0.0); (0.1, 0.01); (0.5, 0.05)}.

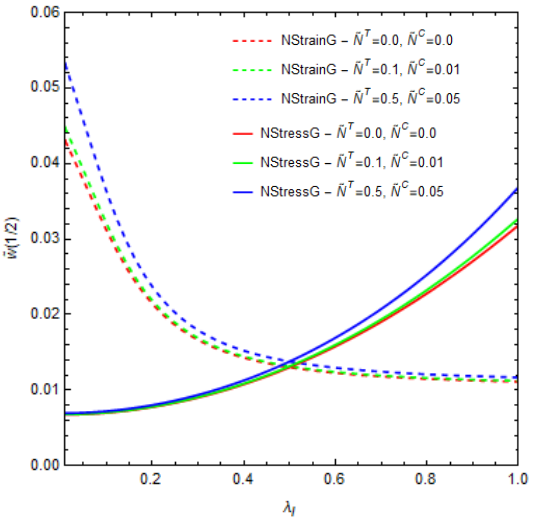

(**a**)

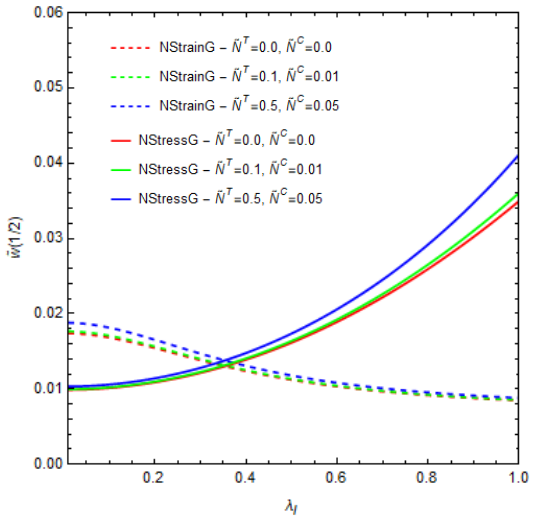

(**b**)

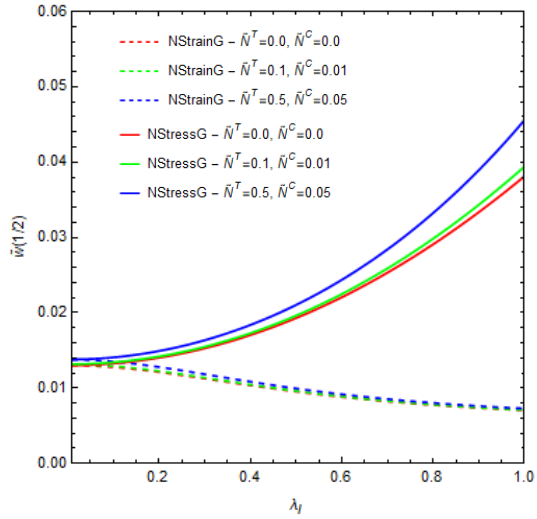

(**c**)

Figures 13(a-c). Simply supported nano-beam under a uniformly distributed load: non-dimensional midpoint deflection $\widetilde{\boldsymbol{w}}(\mathbf{1/2})$ vs. gradient length parameter $\boldsymbol{\lambda_l}$, with the nonlocal parameter $\boldsymbol{\lambda_c = 0.5}$, evaluated by $\boldsymbol{\xi_1 = 0.0}$ (a), $\boldsymbol{\xi_1 = 0.5}$ (b) and $\boldsymbol{\xi_1 = 1.0}$ (c) in NStrainG and NStressG varying $\{\widetilde{\boldsymbol{N}}^{\boldsymbol{T}}, \widetilde{\boldsymbol{N}}^{\boldsymbol{C}}\}$ in the set {(0.0, 0.0); (0.1, 0.01); (0.5, 0.05)}.

Hygro-thermal bending behavior of porous FG nano-beams via local/nonlocal strain and stress gradient theories of elasticity

Rosa PENNA, Luciano FEO, Giuseppe LOVISI

Department of Civil Engineering, University of Salerno, 84084, Fisciano, Italy

TABLES

Table 1. Thermo-elastic properties of metal (*SuS3O4*) and ceramic (*Si3N4*).

Material	Properties	Unit	P_0
Ceramic (*Si3N4*)	E_c	(GPa)	348.40
	ρ_c	(kg/m^3)	2325
	α_c	(K^{-1})	5.8723E-06
	β_c	(wt. % H_2O)$^{-1}$	0
Metal (*SuS3O4*)	E_m	(GPa)	201.04
	ρ_m	(kg/m^3)	8011
	α_m	(K^{-1})	0.00001233
	β_m	(wt. % H_2O)$^{-1}$	0.0005

Table 2. Coefficients of material phases for metal (*SuS3O4*) and ceramic (*Si3N4*).

Coefficients	Unit	Ceramic (*Si3N4*)				Metal (*SuS3O4*)			
		E_c	ρ_c	α_c	β_c	E_m	ρ_m	α_m	β_m
X_{-1}	(K)	0	0	0	0	0	0	0	0
X_1	(K^{-1})	-0.0003070	0	0.0009095	0	0.0003079	0	0.0008086	0
X_2	(K^{-2})	2.160E-07	0	0	0	-6.534E-07	0	0	0
X_3	(K^{-3})	-8.946E-11	0	0	0	0	0	0	0

Table 3. Thermo-elastic properties of metal (*SuS3O4)* and ceramic (*Si3N4*) at different temperatures**.**

Material	**Properties**	**Unit**	**P (305 K)**	**P (405 K)**	**P (505 K)**	**P (605 K)**
Ceramic (*Si3N4*)	E_c	(GPa)	315.80	305.11	294.42	283.74
	ρ_c	(kg/m^3)	2325	2325	2325	2325
	α_c	(K^{-1})	7.501E-06	8.035E-06	8.569E-06	9.104E-06
	β_c	(wt. % H_2O)$^{-1}$	0.00	0.00	0.00	0.00
Metal (*SuS3O4*)	E_m	(GPa)	219.88	226.06	232.23	238.41
	ρ_m	(kg/m^3)	8011	8011	8011	8011
	α_m	(K^{-1})	1.537E-05	1.637E-05	1.737E-05	1.836E-05
	β_m	(wt. % H_2O)$^{-1}$	0.0005	0.0005	0.0005	0.0005

Table 4. Cantilever nano-beam subjected to a concentrated load at the free end: non-dimensional transverse displacement of the free end $\widetilde{\boldsymbol{w}}(\mathbf{1})$ vs. nonlocal parameter $\boldsymbol{\lambda_c}$. Comparison between nonlocal stress gradient (NStressG) and nonlocal strain gradient (NStrainG), assuming $\boldsymbol{\xi_1 = 0.0}$, $\{\widetilde{\boldsymbol{N}}^{\boldsymbol{T}}, \widetilde{\boldsymbol{N}}^{\boldsymbol{C}}\} = \{\mathbf{0.0}, \mathbf{0.0}\}$ and varying $\boldsymbol{\lambda_l}$ in the set (0.0, 0.5).

λ_c	NStrainG				NStressG			
	$\lambda_l = 0.0$	*Ref.[41]*	$\lambda_l = 0.5$	*Ref.[53]*	$\lambda_l = 0.0$	*Ref.[41]*	$\lambda_l = 0.5$	*Ref.[53]*
0^+	0.33333	0.33333	0.27373	0.27373	0.33333	0.33333	0.45833	0.45833
0.1	0.33333	0.33333	0.33804	0.33804	0.28433	0.28433	0.38434	0.38434
0.2	0.33333	0.33333	0.40711	0.40711	0.24101	0.24101	0.31719	0.31719
0.3	0.33333	0.33333	0.48095	0.48095	0.20616	0.20616	0.26329	0.26329
0.4	0.33333	0.33333	0.55956	0.55956	0.17895	0.17895	0.22242	0.22242
0.5	0.33333	0.33333	0.64293	0.64293	0.15758	0.15758	0.19142	0.19142

Table 5. Simply supported nano-beam under uniformly distributed load: non-dimensional midpoint deflection $\widetilde{\boldsymbol{w}}(\mathbf{1/2})$, vs. nonlocal parameter $\boldsymbol{\lambda_c}$. Comparison between nonlocal stress gradient (NStressG) and nonlocal strain gradient (NStrainG), assuming $\boldsymbol{\xi_1 = 0.0}$, $\{\widetilde{\boldsymbol{N}}^{\boldsymbol{T}}, \widetilde{\boldsymbol{N}}^{\boldsymbol{C}}\} = \{\mathbf{0.0}, \mathbf{0.0}\}$ and varying $\boldsymbol{\lambda_l}$ in the set (0.0, 0.5).

λ_c	NStrainG				NStressG			
	$\lambda_l = 0.0$	*Ref.[41]*	$\lambda_l = 0.5$	*Ref.[53]*	$\lambda_l = 0.0$	*Ref.[41]*	$\lambda_l = 0.5$	*Ref.[53]*
0^+	0.01302	0.01302	0.01065	0.01065	0.01302	0.01302	0.04427	0.04427
0.1	0.01471	0.01471	0.01075	0.01075	0.01207	0.01207	0.03592	0.03592
0.2	0.01802	0.01802	0.01103	0.01103	0.01038	0.01038	0.02689	0.02689
0.3	0.02427	0.02427	0.01151	0.01151	0.00888	0.00888	0.02039	0.02039
0.4	0.03302	0.03302	0.01217	0.01217	0.00768	0.00768	0.01602	0.01602
0.5	0.04427	0.04427	0.01302	0.01302	0.00674	0.00674	0.01302	0.01302

Table 6. Cantilever nano-beam subjected to a concentrated load at the free end: non-dimensional transverse displacement of the free end $\widetilde{\boldsymbol{w}}(\mathbf{1})$ vs. nonlocal parameter $\boldsymbol{\lambda_c}$. Comparison between nonlocal stress gradient (NStressG) and nonlocal strain gradient (NStrainG), assuming $\boldsymbol{\xi_1 = 0.0}$, $\{\widetilde{\boldsymbol{N}}^{\boldsymbol{T}}, \widetilde{\boldsymbol{N}}^{\boldsymbol{C}}\} = \{(\mathbf{0.1}, \mathbf{0.01}), (\mathbf{0.5}, \mathbf{0.05})\}$ and varying $\boldsymbol{\lambda_l}$ in the set (0.0, 0.5).

λ_c	$\widetilde{N}^T = 0.1$ - $\widetilde{N}^C = 0.01$				$\widetilde{N}^T = 0.5$ - $\widetilde{N}^C = 0.05$			
	NStrainG		NStressG		NStrainG		NStressG	
	$\lambda_l = 0.0$	$\lambda_l = 0.5$	$\lambda_l = 0.0$	$\lambda_l = 0.5$	$\lambda_l = 0.0$	$\lambda_l = 0.5$	$\lambda_l = 0.0$	$\lambda_l = 0.5$
0^+	0.348383	0.28471	0.348683	0.482952	0.597826	0.33913	0.427674	0.690594
0.1	0.349085	0.35408	0.29586	0.408067	0.609889	0.43718	0.353275	0.514515
0.2	0.350296	0.42973	0.249405	0.333182	0.649192	0.55276	0.289862	0.418436
0.3	0.352332	0.51194	0.212341	0.274173	0.727334	0.69006	0.241319	0.328927
0.4	0.355223	0.60104	0.183618	0.230101	0.874832	0.85488	0.205054	0.267233
0.5	0.359011	0.69737	0.161212	0.197067	1.18376	1.05535	0.177586	0.223569

Table 7. Simply supported nano-beam under uniformly distributed load: non-dimensional midpoint deflection $\widetilde{\boldsymbol{w}}(\mathbf{1/2})$, vs. nonlocal parameter $\boldsymbol{\lambda_c}$. Comparison between nonlocal stress gradient (NStressG) and nonlocal strain gradient (NStrainG), assuming $\boldsymbol{\xi_1 = 0.0}$, $\{\widetilde{\boldsymbol{N}}^{\boldsymbol{T}}, \widetilde{\boldsymbol{N}}^{\boldsymbol{C}}\} = \{(\mathbf{0.1}, \mathbf{0.01}), (\mathbf{0.5}, \mathbf{0.05})\}$ and varying $\boldsymbol{\lambda_l}$ in the set (0.0, 0.5).

λ_c	$\widetilde{N}^T = 0.1$ - $\widetilde{N}^C = 0.01$				$\widetilde{N}^T = 0.5$ - $\widetilde{N}^C = 0.05$			
	NStrainG		NStressG		NStrainG		NStressG	
	$\lambda_l = 0.0$	$\lambda_l = 0.5$	$\lambda_l = 0.0$	$\lambda_l = 0.5$	$\lambda_l = 0.0$	$\lambda_l = 0.5$	$\lambda_l = 0.0$	$\lambda_l = 0.5$
0^+	0.01317	0.01075	0.01317	0.04606	0.01379	0.01117	0.01379	0.05495
0.1	0.01445	0.01085	0.01219	0.03709	0.01521	0.01128	0.01273	0.04264
0.2	0.01831	0.01114	0.01047	0.02753	0.01955	0.01159	0.01087	0.03042
0.3	0.02480	0.01162	0.00895	0.02075	0.02715	0.01211	0.00923	0.02235
0.4	0.03401	0.01230	0.00773	0.01625	0.03861	0.01284	0.00795	0.01721
0.5	0.04606	0.01317	0.00678	0.01317	0.05495	0.01379	0.00695	0.01379

Table 8. Cantilever nano-beam subjected to a concentrated load at the free end: non-dimensional transverse displacement of the free end $\widetilde{\boldsymbol{w}}(\mathbf{1})$ vs. gradient length parameter $\boldsymbol{\lambda_l}$, with the nonlocal parameter $\boldsymbol{\lambda_c = 0.5}$, evaluated by $\boldsymbol{\xi_1 = 0.0}$ in NStrainG and NStressG varying $\{\widetilde{\boldsymbol{N}}^{\boldsymbol{T}}, \widetilde{\boldsymbol{N}}^{\boldsymbol{C}}\}$ in the set {(0.0, 0.0); (0.1, 0.01); (0.5, 0.05)}.

λ_l	*Present approach*						*Ref. [53]*	
	$\widetilde{N}^T = 0.0 - \widetilde{N}^C = 0.0$		$\widetilde{N}^T = 0.1 - \widetilde{N}^C = 0.01$		$\widetilde{N}^T = 0.5 - \widetilde{N}^C = 0.05$		$\widetilde{N}^T = 0.0 - \widetilde{N}^C = 0.0$	
	NStrainG	NStressG	NStrainG	NStressG	NStrainG	NStressG	NStrainG	NStressG
0^+	1.08333	0.15758	1.23930	0.16121	2.79020	0.17759	1.08333	0.24546
0.1	0.97534	0.15894	1.09899	0.16264	2.23806	0.17937	0.97534	0.24681
0.2	0.86180	0.16300	0.95868	0.16692	1.74592	0.18475	0.86180	0.25087
0.3	0.76428	0.16976	0.98406	0.17408	1.40101	0.19381	0.76428	0.25764
0.4	0.69260	0.17924	0.75545	0.18412	1.18712	0.20668	0.69260	0.26411
0.5	0.64293	0.19142	0.69737	0.19707	1.05535	0.22357	0.64293	0.27929
0.6	0.60871	0.20630	0.65778	0.21297	0.97141	0.24475	0.60871	0.29418
0.7	0.58475	0.22390	0.63026	0.23185	0.91564	0.27058	0.58475	0.31177
0.8	0.56756	0.24420	0.61063	0.25377	0.87710	0.30152	0.56756	0.33207
0.9	0.55494	0.26720	0.59626	0.16121	0.84952	0.17759	0.55494	0.35508
1.0	0.54545	0.15758	0.58550	0.16264	0.82917	0.17937	0.54545	0.38079

Table 9. Cantilever nano-beam subjected to a concentrated load at the free end: non-dimensional transverse displacement of the free end $\widetilde{\boldsymbol{w}}(\mathbf{1})$ vs. gradient length parameter $\boldsymbol{\lambda_l}$, with the nonlocal parameter $\boldsymbol{\lambda_c = 0.5}$, evaluated by $\boldsymbol{\xi_1 = 0.5}$ in NStrainG and NStressG varying $\{\widetilde{\boldsymbol{N}}^{\boldsymbol{T}}, \widetilde{\boldsymbol{N}}^{\boldsymbol{C}}\}$ in the set {(0.0, 0.0); (0.1, 0.01); (0.5, 0.05)}.

λ_l	*Present approach*						*Ref. [53]*	
	$\widetilde{N}^T = 0.0 - \widetilde{N}^C = 0.0$		$\widetilde{N}^T = 0.1 - \widetilde{N}^C = 0.01$		$\widetilde{N}^T = 0.5 - \widetilde{N}^C = 0.05$		$\widetilde{N}^T = 0.0 - \widetilde{N}^C = 0.0$	
	NStrainG	NStressG	NStrainG	NStressG	NStrainG	NStressG	NStrainG	NStressG
0^+	0.46003	0.24546	0.48902	0.25388	0.65471	0.29435	0.46003	0.24546
0.1	0.45720	0.24681	0.48577	0.25535	0.64833	0.29643	0.45720	0.24681
0.2	0.44917	0.25087	0.47655	0.25975	0.63084	0.30271	0.44917	0.25087
0.3	0.43743	0.25764	0.46321	0.26710	0.60657	0.31328	0.43743	0.25764
0.4	0.42415	0.26411	0.44825	0.27743	0.58047	0.32832	0.42415	0.26411
0.5	0.41114	0.27929	0.43371	0.29074	0.55597	0.34810	0.41114	0.27929
0.6	0.39945	0.29418	0.42071	0.30709	0.53468	0.37297	0.39945	0.29418
0.7	0.38944	0.31177	0.40962	0.32651	0.51691	0.40339	0.38944	0.31177
0.8	0.38106	0.33207	0.40038	0.34906	0.50237	0.43996	0.38106	0.33207
0.9	0.37415	0.35508	0.39277	0.37480	0.49055	0.48345	0.37415	0.35508
1.0	0.36845	0.38079	0.38652	0.40379	0.48095	0.53487	0.36845	0.38079

Table 10. Cantilever nano-beam subjected to a concentrated load at the free end: non-dimensional transverse displacement of the free end $\widetilde{\boldsymbol{w}}(\mathbf{1})$ vs. gradient length parameter $\boldsymbol{\lambda_l}$, with the nonlocal parameter $\boldsymbol{\lambda_c = 0.5}$, evaluated by $\boldsymbol{\xi_1 = 1.0}$ in NStrainG and NStressG varying $\{\widetilde{\boldsymbol{N}}^{\boldsymbol{T}}, \widetilde{\boldsymbol{N}}^{\boldsymbol{C}}\}$ in the set {(0.0, 0.0); (0.1, 0.01); (0.5, 0.05)}.

λ_l	*Present approach*						*Ref. [53]*	
	$\widetilde{N}^T = 0.0$ - $\widetilde{N}^C = 0.0$		$\widetilde{N}^T = 0.1$ - $\widetilde{N}^C = 0.01$		$\widetilde{N}^T = 0.5$ - $\widetilde{N}^C = 0.05$		$\widetilde{N}^T = 0.0$ - $\widetilde{N}^C = 0.0$	
	NStrainG	NStressG	NStrainG	NStressG	NStrainG	NStressG	NStrainG	NStressG
0^+	0.33333	0.33333	0.34868	0.34868	0.42767	0.42767	0.33333	0.33333
0.1	0.33200	0.33469	0.34720	0.35019	0.42528	0.43012	0.33200	0.33469
0.2	0.32823	0.33875	0.34302	0.35472	0.41860	0.43750	0.32823	0.33875
0.3	0.32264	0.34551	0.33684	0.36228	0.40893	0.44995	0.32264	0.34551
0.4	0.31601	0.35499	0.32954	0.37290	0.39776	0.46770	0.31601	0.35499
0.5	0.30905	0.36717	0.32192	0.38660	0.38634	0.49108	0.30905	0.36717
0.6	0.30230	0.38205	0.31455	0.40341	0.37551	0.52056	0.30230	0.38205
0.7	0.29606	0.39965	0.30777	0.42339	0.36570	0.55675	0.29606	0.39965
0.8	0.29048	0.41995	0.30173	0.44658	0.35708	0.60044	0.29048	0.41995
0.9	0.28559	0.44296	0.29644	0.47306	0.34962	0.65268	0.28559	0.44296
1.0	0.28135	0.46867	0.29187	0.50290	0.34324	0.71479	0.28135	0.46867

Table 11. Simply supported nano-beam under uniformly distributed: non-dimensional midpoint deflection $\widetilde{\boldsymbol{w}}(\mathbf{1/2})$ vs. gradient length parameter $\boldsymbol{\lambda_l}$, with the nonlocal parameter $\boldsymbol{\lambda_c = 0.5}$, evaluated by $\boldsymbol{\xi_1 = 0.0}$ in NStrainG and NStressG varying $\{\widetilde{\boldsymbol{N}}^{\boldsymbol{T}}, \widetilde{\boldsymbol{N}}^{\boldsymbol{C}}\}$ in the set {(0.0, 0.0); (0.1, 0.01); (0.5, 0.05)}.

λ_l	*Present approach*						*Ref. [53]*	
	$\widetilde{N}^T = 0.0 - \widetilde{N}^C = 0.0$		$\widetilde{N}^T = 0.1 - \widetilde{N}^C = 0.01$		$\widetilde{N}^T = 0.5 - \widetilde{N}^C = 0.05$		$\widetilde{N}^T = 0.0 - \widetilde{N}^C = 0.0$	
	NStrainG	NStressG	NStrainG	NStressG	NStrainG	NStressG	NStrainG	NStressG
0^+	0.04427	0.00674	0.04606	0.00678	0.05495	0.00695	0.04427	0.00674
0.1	0.03118	0.00700	0.03209	0.00704	0.03635	0.00721	0.03118	0.00700
0.2	0.02146	0.00775	0.02187	0.00780	0.02370	0.00822	0.02146	0.00775
0.3	0.01665	0.00900	0.01689	0.00907	0.01794	0.00937	0.01665	0.00900
0.4	0.01429	0.01076	0.01447	0.01086	0.01522	0.01128	0.01429	0.01076
0.5	0.01302	0.01302	0.01317	0.01317	0.01379	0.01379	0.01302	0.01302
0.6	0.01228	0.01578	0.01241	0.01600	0.01296	0.01693	0.01228	0.01578
0.7	0.01181	0.01905	0.01193	0.01936	0.01244	0.02074	0.01181	0.01905
0.8	0.01149	0.02281	0.01161	0.02327	0.01210	0.02529	0.01149	0.02281
0.9	0.01127	0.02708	0.01139	0.02779	0.01185	0.03064	0.01127	0.02708
1.0	0.01112	0.03185	0.01122	0.03275	0.01168	0.03690	0.01112	0.03185

Table 12. Simply supported nano-beam under uniformly distributed: non-dimensional midpoint deflection $\widetilde{\boldsymbol{w}}(\mathbf{1/2})$ vs. gradient length parameter $\boldsymbol{\lambda_l}$, with the nonlocal parameter $\boldsymbol{\lambda_c = 0.5}$, evaluated by $\boldsymbol{\xi_1 = 1.0}$ in NStrainG and NStressG varying $\{\widetilde{\boldsymbol{N}}^{\boldsymbol{T}}, \widetilde{\boldsymbol{N}}^{\boldsymbol{C}}\}$ in the set {(0.0, 0.0); (0.1, 0.01); (0.5, 0.05)}.

λ_l	*Present approach*						*Ref. [53]*	
	$\widetilde{N}^T = 0.0 - \widetilde{N}^C = 0.0$		$\widetilde{N}^T = 0.1 - \widetilde{N}^C = 0.01$		$\widetilde{N}^T = 0.5 - \widetilde{N}^C = 0.05$		$\widetilde{N}^T = 0.0 - \widetilde{N}^C = 0.0$	
	NStrainG	NStressG	NStrainG	NStressG	NStrainG	NStressG	NStrainG	NStressG
0^+	0.01741	0.00988	0.01767	0.00997	0.01882	0.01032	0.01741	0.00988
0.1	0.01684	0.01013	0.01708	0.01022	0.01815	0.01060	0.01684	0.01013
0.2	0.01544	0.01089	0.01565	0.01099	0.01654	0.01142	0.01544	0.01089
0.3	0.01383	0.01214	0.01400	0.01227	0.01470	0.01281	0.01383	0.01214
0.4	0.01238	0.01390	0.01252	0.01407	0.01308	0.01478	0.01238	0.01390
0.5	0.01123	0.01616	0.01133	0.01639	0.01179	0.01736	0.01123	0.01616
0.6	0.01034	0.01892	0.01044	0.01923	0.01082	0.02059	0.01034	0.01892
0.7	0.00968	0.02219	0.00976	0.02262	0.01010	0.02452	0.00968	0.02219
0.8	0.00917	0.02595	0.00925	0.02654	0.00955	0.02920	0.00917	0.02595
0.9	0.00879	0.03022	0.00989	0.03102	0.00913	0.03472	0.00879	0.03022
1.0	0.00849	0.03499	0.00855	0.03607	0.00881	0.04118	0.00849	0.03499

Table 13. Simply supported nano-beam under uniformly distributed: non-dimensional midpoint deflection $\widetilde{\boldsymbol{w}}(\mathbf{1/2})$ vs. gradient length parameter $\boldsymbol{\lambda_l}$, with the nonlocal parameter $\boldsymbol{\lambda_c = 0.5}$, evaluated by $\boldsymbol{\xi_1 = 1.0}$ in NStrainG and NStressG varying $\{\widetilde{\boldsymbol{N}}^{\boldsymbol{T}}, \widetilde{\boldsymbol{N}}^{\boldsymbol{C}}\}$ in the set {(0.0, 0.0); (0.1, 0.01); (0.5, 0.05)}.

λ_l	*Present approach*						*Ref. [53]*	
	$\widetilde{N}^T = 0.0 - \widetilde{N}^C = 0.0$		$\widetilde{N}^T = 0.1 - \widetilde{N}^C = 0.01$		$\widetilde{N}^T = 0.5 - \widetilde{N}^C = 0.05$		$\widetilde{N}^T = 0.0 - \widetilde{N}^C = 0.0$	
	NStrainG	NStressG	NStrainG	NStressG	NStrainG	NStressG	NStrainG	NStressG
0^+	0.01302	0.01302	0.01317	0.01317	0.01379	0.01379	0.01302	0.01302
0.1	0.01278	0.01327	0.01292	0.01343	0.01352	0.01407	0.01278	0.01327
0.2	0.01213	0.01403	0.01226	0.01420	0.01280	0.01492	0.01213	0.01403
0.3	0.01127	0.01528	0.01138	0.01548	0.01184	0.01635	0.01127	0.01528
0.4	0.01037	0.01704	0.01046	0.01729	0.01085	0.01838	0.01037	0.01704
0.5	0.00954	0.01930	0.00962	0.01962	0.00995	0.02104	0.00954	0.01930
0.6	0.00883	0.02206	0.00890	0.02249	0.00918	0.02437	0.00883	0.02206
0.7	0.00824	0.02532	0.00830	0.02589	0.00855	0.02841	0.00824	0.02532
0.8	0.00776	0.02909	0.00782	0.02983	0.00803	0.03324	0.00776	0.02909
0.9	0.00738	0.03336	0.00742	0.03434	0.00762	0.03894	0.00738	0.03336
1.0	0.00706	0.03813	0.00711	0.03942	0.00729	0.04559	0.00706	0.03813